Correlating Cochlear Morphometrics from Parnell's Mustached Bat (*Pteronotus parnellii*) with Hearing

Cassandra D. Girdlestone[1], Jodie Ng[1], Manfred Kössl[3], Adrien Caplot[2], Robert E. Shadwick[1], and Maria Morell[1,2,4]

[1]Department of Zoology, University of British Columbia, Vancouver, BC V6T 1Z4, Canada. (Cassandra Girdlestone: cassgird@zoology.ubc.ca; Jodie Ng: jodie.ng@alumni.ubc.ca; Robert E. Shadwick: shadwick@zoology.ubc.ca).

[2]INSERM-UMR 1051, Institute for Neurosciences of Montpellier, 34091 Montpellier, France. (Adrien Caplot: adrien.caplot@inserm.fr, Maria Morell: maria.morell@tiho-hannover.de).

[3]Institute for Cell Biology and Neuroscience, Goethe University, 60438 Frankfurt/Main, Max-von-Laue Str.13. (koessl@bio.uni-frankfurt.de).

[4]Institute for Terrestrial and Aquatic Wildlife Research, University of Veterinary Medicine Hannover, Foundation, 25761, Bsum, Germany.

Short title:

Bat cochlear morphometrics

Corresponding author: C.D. Girdlestone (email: cassgird@zoology.ubc.ca).

Word Counts:

Introduction: 930

Discussion: 2123

Tables: 4 (two in the main text, plus two supplementary tables)

Figures: 11

Abstract

Morphometric analysis of the inner ear of mammals can provide information for cochlear frequency mapping, a species-specific designation of locations in the cochlea at which different sound frequencies are encoded. Morphometric variation occurs in the hair cells of the organ of Corti along the cochlea, with the base encoding the highest frequency sounds and the apex encoding the lowest frequencies. Changes in cell shape and spacing can yield additional information about the biophysical basis of cochlear tuning mechanisms. Here, we investigate how morphometric analysis of hair cells in mammals can be used to predict the relationship between frequency and cochlear location. We used linear and geometric morphometrics to analyze scanning electron micrographs of the hair cells of the cochleae in Parnell's mustached bat (*Pteronotus parnellii*) and Wistar rat (*Rattus norvegicus*) and determined a relationship between cochlear morphometrics and their frequency map. Sixteen of twenty-two of the morphometric parameters analyzed showed a significant change along the cochlea, including the distance between the rows of hair cells, outer hair cell width, and gap width between hair cells. A multiple linear regression model revealed that nine of these parameters are responsible for 86.9% of the variation in these morphometric data. Determining the most biologically relevant measurements related to frequency detection can give us a greater understanding of the essential biomechanical characteristics for frequency selectivity during sound transduction in a diversity of animals.

Key words:

inner ear; organ of Corti; geometric morphometrics; linear morphometrics; frequency map

Introduction

Many morphological and biomechanical features of the inner ear have been conserved across different species of terrestrial placental mammals (Echteler et al. 1994; Vater and Kössl 2011) but there is still a great deal of variation in hearing capability to investigate (i.e. generalists versus high-frequency specialists). In mammals we still do not know what determines the specific frequency response of each cochlear location. How do we distinguish between correlations relating frequency with anatomy, and the possibility that the morphological features are really causal of the frequency response?

Within the inner ear is a spiral-shaped structure known as the cochlea. The cochlea is comprised of three fluid-filled ducts or channels. The center-most of these channels is where the organ of Corti, the hearing organ, is located. The surface of the organ of Corti reveals an arrangement of two types of sensory cells, the inner hair cells (IHCs) and the outer hair cells (OHCs). Typically, for placental mammals, the IHCs are organized in a single row, while the OHCs form three parallel rows (Lim 1986). OHCs play a crucial role in frequency selectivity and increasing sensitivity, while IHCs are responsible for the transduction of the mechanical stimulus into an electrical signal (for a review, see Fettiplace and Kim 2014). The shape and spacing of the OHC stereociliary bundles affect the flow of the fluid surrounding the stereocilia that in turn stimulates the stereocilia of the IHCs. To further understand the biophysical relationship between morphology and frequency sensitivity, additional modelling is necessary. Morphological measurements of the various parameters of the reticular lamina and stereociliary bundles could add to research in this area (Pau and Pau 2006; Guinan 2012; Ni et al. 2016; Ciganović et al. 2017). Analyzing variations in the morphology of the reticular lamina and stereociliary bundles of sensory hair cells across species, as a function of the frequencies that are encoded along the cochlear length, will provide novel and critically important information that could be

incorporated into biophysical models of cochlear dynamics (Lim and Steele 2002; Ni et al. 2016; Ciganović et al. 2017). Comparative studies may help improve our understanding of frequency sensitivity in cochlear hair cells. In particular, a focus on the specific structures contributing to sound reception and processing within the inner ear would be beneficial for assessing similarities between species with different but overlapping hearing ranges.

Studies of inner ear physiology have given us a wealth of information about many characteristics of the organ of Corti including biomechanics of the basilar membrane and hair cells (Von Békésy 1960; Dallos 1992), and the innervation of the hair cells (Raphael and Altschuler 2003). Morphometric analysis of the reticular lamina and stereociliary bundles of the guinea pig (Yarin et al. 2014) shows variation in the microstructures of these cells with respect to location and the frequency encoded by these cells. Other frequency-related features include the length of the OHC bodies (i.e. maximal length of the basolateral membrane on a modiolar transverse section of the cochlea, Dannhof et al. 1991; Pujol et al. 1992), the length of the supporting cells (Spicer and Schulte 1994), the area occupied by the cells of the organ of Corti (as viewed in cross-section perpendicularly from the reticular lamina to the basilar membrane), and the diameter of the fibers of the basilar membrane (Schweitzer et al. 1996). Furthermore, it is crucial to have information on the height of the tallest stereocilia, the distance between stereociliary bundles, and the inner angle between the arms of the stereociliary bundles along the cochlear spiral to be able to model energy flow in the longitudinal and lateral directions of the organ of Corti (Pau and Pau 2006; Guinan 2012; Ni et al. 2016; Ciganović et al. 2017).

The goal of our study is to investigate whether a relationship exists between the morphometrics of the cuticular plate (the apical portion of the cell) and encoding frequencies, across species. Mammals have many hearing differences, yet the mechanistic basis of hearing and cochlear structure are common among all (Echteler et al. 1994). Mammals that echolocate

emit and receive higher frequencies than non-echolocating mammals. Parnell's mustached bat hears frequencies from 10 kHz to 112 kHz (Kössl 1994a; Kössl and Vater 1996) and has an established cochlear frequency map (Kössl and Vater 1985). In addition, the organ of Corti of Parnell's mustached bat has been thoroughly described in previous research encompassing otoacoustic emissions, calculation and description of the cochlear frequency map, and the ultrastructure of the cochlea (Kössl 1994b; Kössl and Vater 1985; Vater and Kössl 1996). To determine if these linear morphometric analyses are comparable across mammalian species, we looked at another species that has a well-documented frequency map. Wistar rats were selected since their hearing range (1.2 – 54 kHz, Müller 1991) overlaps with the lower end of the bat hearing range, but they also hear well below the range of bats. This makes both species suitable for combining morphometric analyses with known frequency data to generate a predictive relationship between morphology and frequency along the cochlea. Combining the morphometric information for both species can give a frequency map that extends beyond the hearing range of each species, and this could be a proxy for other placental mammals that have broader hearing ranges.

In this study, we analyzed scanning electron micrographs of the cochlear hair cells in Parnell's mustached bats (*Pteronotus parnellii*) and Wistar rats (*Rattus norvegicus*), using both linear (LM) and geometric morphometric (GM) techniques. We then constructed a multiple linear regression model to predict frequency encoding of other species based on our results and the known frequency maps of bats and rats.

Methods

Extraction and fixation

Cochlear samples from the inner ears of Parnell's mustached bat (*Pteronotus parnellii*) (Fig. 1a), were collected from six adult individuals (from the Cuban population). These bats were originally imported live from Cuba to Germany with all required export and import permits, for use in research, separate from that described here, on cochlear function. As required by governmental animal experimentation control agencies in Germany, these bats were euthanized by administering pentobarbital intraperitoneally at a dose of 400 mg/kg. We processed the cochleae of four males and two females, ranging in weight from 10 to 13g and forearm length of 50.5 to 51.5 mm. Only one cochlea per bat was analyzed, except for one individual in which both cochleae were measured. However, we averaged the data from this individual. Three of these cochleae were from left ears, while four were from right ears (n = 6). The animals received intracardial perfusions at a rate of 4 ml/minute for five minutes with 0.9% NaCl, and for thirty minutes with 4% paraformaldehyde in 0.1 M phosphate buffer to fix the inner ear. The Institute of Cell Biology and Neuroscience, Goethe University, Germany provided these samples that, after fixation, were shipped to the University of British Columbia, Vancouver, British Columbia, Canada for further laboratory analysis. All experiments described herein were carried out in accordance with current laws for animal experimentation in Germany (Regierungspräsidium Darmstadt) and according to the Declaration of Helsinki.

Four Wistar rats (*Rattus norvegicus*) were decapitated under deep anesthesia (pentobarbital, 50 mg/kg) and their cochleae were removed from the temporal bone and fixed with 3.5% glutaraldehyde in 0.1 M phosphate buffer (pH 7.3) at room temperature. Cochleae were first perfused with the fixative in turn through both the round and oval windows and then immersed in the fixative for at least one hour. A hole made in the bone at the apex of the cochlea

provided an exit point for the fixative solution. Marc Lenoir from the Institute for Neurosciences of Montpellier provided and dissected the rat cochleae. Experiments were carried out in accordance with the animal welfare guidelines of the Institut National de la Santé et de la Recherche Médicale and approved by the French Ministère de l'Agriculture et de la Forêt.

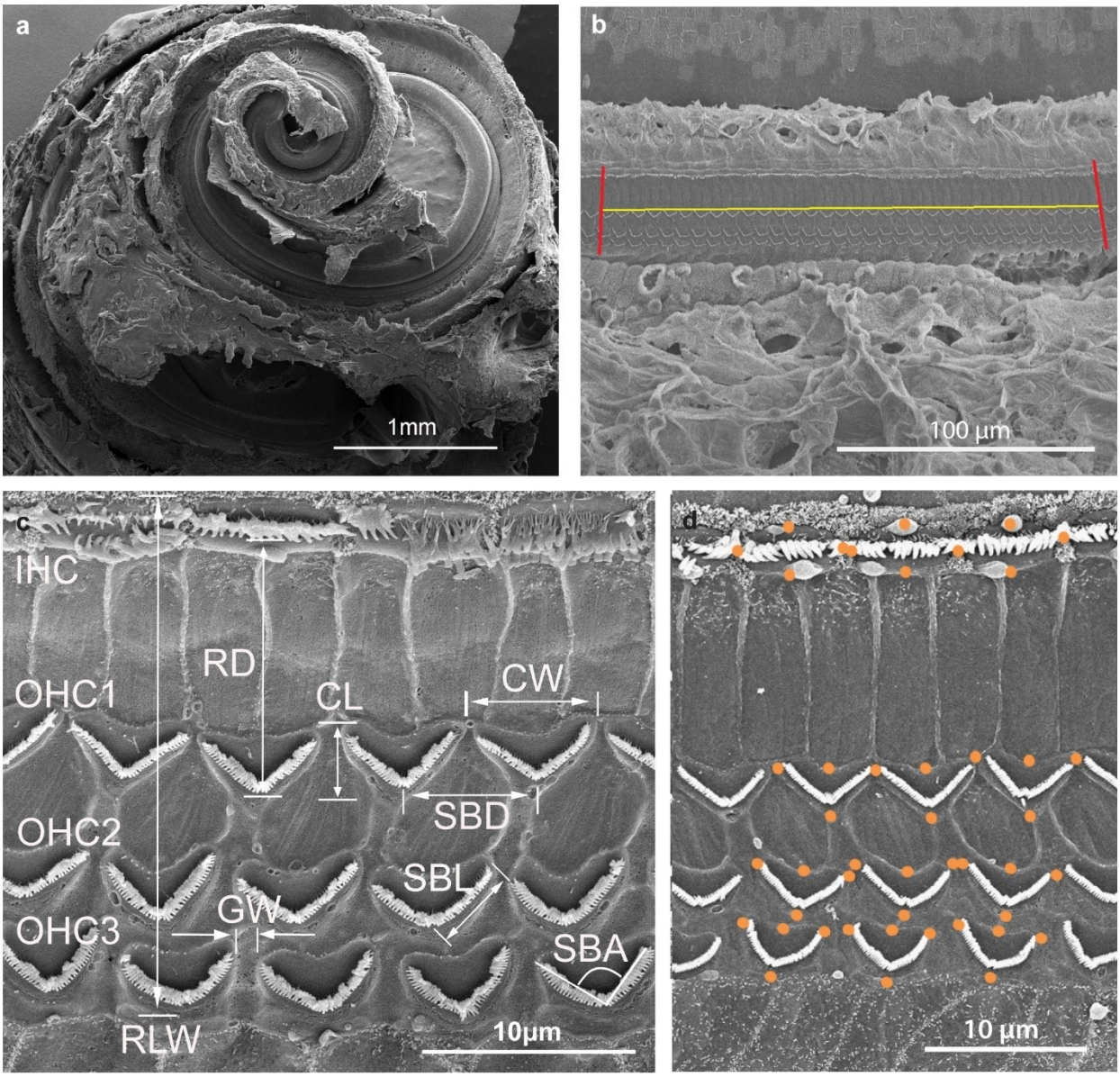

Figure 1. Scanning electron micrographs of the cochlea and the organ of Corti of Parnell's mustached bat. (a) Parnell's mustached bat cochlea. (b) Surface of the organ of Corti showing the measurements made in each consecutive image to calculate the cochlear length. (c) Surface of the organ of Corti in a bat cochlea, showing the typical arrangement of the hair cells. Visible here is the single row

of inner hair cells (IHC) as well as the three parallel rows of outer hair cells (OHC1, OHC2, and OHC3). Measurements shown are the parameters analyzed (RLW) distance from inner hair cells to the third row of outer hair cells (width of the reticular lamina), (RD) distance between the rows of hair cells, (CL) cuticular plate length of the outer hair cells, (CW) cuticular plate width of the outer hair cells, (SBD) distance between the stereociliary bundle tips, (GW) gap width between outer hair cells, (SBL) stereociliary bundle side arm length, and (SBA) inner angle of the stereociliary bundles of the outer hair cells (Table 1). (d) The landmarks used for the geometric morphometric analysis are shown as orange dots to demarcate the shape of the hair cells.

Decalcification

After the samples were fixed, the periotic bone that surrounds the cochlea in the bats was decalcified to the point at which the scala vestibuli and the stria vascularis were visible. Decalcification took place over a period of 13 hours, using 14% EDTA tetrasodium salt (pH 7.4) as described by Morell and colleagues (2015, 2017). The cochleae of the rats were not decalcified.

Scanning electron microscopy – dissection and processing

The cochlear samples were dissected with the scala vestibuli and the stria vascularis cut open, and both Reissner's and tectorial membranes removed, to access the reticular lamina and stereociliary bundles of the organ of Corti. Dehydration of the samples was then carried out using gradually increasing concentrations of ethanol up to 100%. Once dehydrated, the cochlear samples were critical point dried using CO_2 and sputter coated with either gold-palladium or platinum-palladium. This was done in preparation for imaging in a Hitachi S-4700 scanning electron microscope (SEM) at the University of British Columbia Bioimaging Facility,

Vancouver, British Columbia, Canada, and a Hitachi S-4000 (COMET, Montpellier Resources Imagery) SEM.

Image analysis and morphometry

SEM micrographs were adjusted for brightness and contrast using Adobe Photoshop® CS3. Measurements of the cochlear structures were made using ImageJ® version 1.51j8 software (Schneider et al. 2012).

Cochlear lengths were calculated for the mustached bats (n = 6) and rats (n = 4) along the limit between the first row of OHCs and the inner pillar cells (Fig. 1b). An average of 43 flat SEM micrographs were measured per bat cochlea and an average of 24 flat SEM micrographs per rat cochlea. The cochleae were tilted under the microscope to obtain a flat micrograph from a spiral structure. In order to calculate the cochlear length, the images were organized sequentially. In each micrograph, distinguishing features were used to demarcate the length to be measured in each consecutive image, to ensure that there were no overlapping sections or gaps between sections (Fig. 1b). These measurements were then totaled to calculate the cochlear length of each sample.

LM measurements of the cochlear structures were made using ImageJ© software, while GM measurements were acquired using tpsUtil, tpsDig2 (Rohlf 2004a, 2004b), and MorphoJ© (Klingenberg 2011) software. Additional analyses of the GM measurements were performed in R 3.5.0. using the geomorph package (Adams et al. 2018).

Linear morphometric analysis

LM measurements were obtained from the cochleae of mustached bats (n = 6) and rats (n = 4). These measurements were taken using the same procedure in both species. Following

methods used in recent LM analysis (Yarin et al., 2014), we measured eight parameters of the IHCs and the OHCs, as well as the height of the stereocilia of the OHCs (n = 25 total parameters). These parameters are shown in Fig. 1c and detailed in Table 1. Depending on the row in which the cells were measured, each parameter has three designations, for example, parameter GW – mean gap width, is comprised of GW1, GW2, and GW3 (Table 1).

Table 1. Summary of parameters measured using linear morphometrics, showing the designated cell row in which measurements were taken. IHC: inner hair cell, OHC: outer hair cell.

Parameter	Abbreviation	Outer Hair Cell Row Designation
Width of the reticular lamina	RLW	Distance from IHC - OHC3
Distance between rows of hair cells	RD1 RD2 RD3	Distance from IHC-OHC1 Distance from OHC1-OHC2 Distance from OHC2-OHC3
Outer hair cell length	CL1 CL2 CL3	1 2 3
Outer hair cell width	CW1 CW2 CW3	1 2 3
Distance between stereociliary bundle tips	SBD1 SBD2 SBD3	1 2 3
Gap width between outer hair cells	GW1 GW2 GW3	1 2 3
Stereociliary bundles - side arm length	SBL1 SBL2 SBL3	1 2 3
Stereociliary bundles - inner angle	SBA1 SBA2 SBA3	1 2 3

The exact locations at which these parameters were measured varied within our cochlear samples. This variation resulted from the condition of the organ of Corti samples and the ability to take images at each location due to the angle of the region because of the curvature of the

cochlea. In the analyses and graphing of these data, points covering a small range of locations were grouped to obtain average values. From 0% up to 10% of the distance along the cochlear length, data were grouped by a single percent (i.e. 0-1%, 1-2%, and so on) since this is the region of the cochlea where the highest morphological variation is observed. From the distance of 10% to 100%, data points were averaged in a range of five percent (i.e. 10-15%, 15-20%, etc.). Multiple measurements were taken of individual cell parameters from each row of OHCs, at each location. In the mustached bat cochlear samples, 5 to 13 locations were analyzed in each of the cochleae. These locations covered the area of the organ of Corti from 0.4% to 99.1% distance from the apex. The cochlear samples from the rat had LMs analyzed at ten locations along the cochlea, reaching from the apex to a distance along the cochlear length of 95% from the apex.

We analyzed the measurements, then compared the results for seven of the parameters that showed the greatest changes associated with the location (% distance from the apex) along the organ of Corti.

In addition to the parameters described above, the height of the stereocilia were also measured in the mustached bats. Our methodology differed from that of Yarin and colleagues (2014) who used two images, knowing the angular difference between the two, to calculate a "true height". In our analysis, we initially attempted to replicate this method. We found that when we compared this measurement to the height of the stereocilia imaged straight on, from a viewpoint parallel to the stereocilia, and having a flat image of the stereocilia – there was no significant difference in the heights. Therefore, moving forward we took just one image per area for analysis and measured the height as the distance from base to tip of the individual stereocilia.

The cochlear measurements for the LM analyses were also analyzed using statistical modelling, in which the computer uses algorithms to "learn" patterns based on sample data entered (relating morphometry with coding frequency in our case) and by running numerous

repetitions (El Naqa and Murphy 2015). At this point, novel data can be introduced and analyzed. We did not perform any transformation of these data prior to analysis. The advantage of using statistical modelling relies on the possibility of extracting those variables that explain the majority of the variance in large datasets with numerous variables. As a result, we can predict the frequency of a new location in the cochlea by measuring only certain variables. Since there are multiple variables for each parameter measured, we used a stepwise model selection by Akaike Information Criterium with a correction for small sample sizes (AICc) to select the best or most relevant parameters to analyze further (Burnhan and Anderson 2002). Data from nine parameters were then used to create a linear model from which frequency maps for other species can be calculated if morphometric data are available. Statistical analysis was programmed and performed with R software (version 3.4.4) (R Core Team 2018). The R package MuMIn was used for the AICc analyses (Barton 2019).

The statistical analysis of data from the bats and rats was initially carried out separately. The normality of the data of the hair cells in the apex (0-10%) and in the base (90-100%) was evaluated using a Shapiro-Wilk test. When the data followed a normal distribution ($W \approx 1$, p value > 0.05) we applied a T-test to analyze the variance of our data comparing the hair cells at the apex to those at the base to determine the total overall change. When the data did not follow a normal distribution (i.e. parameters other than RD2, CL1, CW2, and CW3 for bats and all parameters except for CL3, CW1, CW2, CW3, SBD1, SBD2, and SBD3 for rats), we applied a Wilcoxon test to compare the hair cells at the apex with those at the base (see above). For several parameters where we did not observe a clear trend between the apex and the base, or when we observed an irregular pattern in the representation of the data in the center regions (average of the three rows for CW, SBD and SBA) we did some additional statistics between the region of 35-100% (the classes were: 35-50%, 50-70%, and 70-100%). For this region of 35-100% in CW,

SBD and SBA, we applied a Kruskal-Wallis test, and a Dunn´s post-hoc test since the data did not follow a normal distribution.

Geometric morphometric analysis

GMs were used for the mustached bats (n = 6) and rats (n = 4). Using the software tpsDig2 cells were digitized in blocks of 12 cells (three IHCs and nine OHCs, consisting of three OHCs in each of the three rows) (Fig. 1d). These groups of cells were separated into individual cells during these analyses. The four landmarks chosen per cell (Table S1 and Fig. 1d) were selected to capture the variation in the hair cell shapes. These measurements were taken from 10 locations along the length of the cochleae, spaced apart at increments of 10% (± 2%) of the cochlear length from 5% to 95%. We chose the same locations in both species to have a representation of the organ of Corti all along the cochlear spiral and to be able to then analyze our data using MorphoJ©. As described earlier, due to the condition of the organ of Corti at the various locations and the angle of the surface with respect to the SEM lens, not all locations could be analyzed in each cochlea. Having selected and digitized 48 landmarks for each group or block of IHCs and OHCs (Fig. 1d, and Table S1) for at least three replicates per location, we then performed a Procrustes fit using MorphoJ©. Following this preliminary step, we then performed three principal component analyses (PCAs) (Jolliffe 2002). First, we analyzed the IHCs and OHCs together in a block of 12 cells (3 IHC and 9 OHC). Next, the digitized cells were split into two groups and analyzed separately as IHCs and OHCs to determine whether the shape variation of a specific hair cell type could be linked to the location. Finally, the OHCs were isolated and the PCs and were analyzed to see how the shapes changed among these cells separately from the IHCs. Additionally, we plotted PC1 of the OHCs as a function of frequency

and corresponding to location along the cochlear length. Finally, for these GM data from the IHCs and OHCs, we performed a regression analysis of the hair cell shape onto frequency.

Results

Linear morphometric analysis in the mustached bat

Mean cochlear length of mustached bats (n = 6) ranged from 8.90 mm to 11.68 mm with an average of 10.53 mm. As in other terrestrial mammals, there was visible variation in the hair cell spacing and morphometric parameters from the apex to the base.

Not all of the 22 measured parameters with LM changed with respect to their position along the cochlear length, and the parameters represented in Fig 2 showed the most variation. Table S2 shows a summary of all the results from the statistical analysis. The LM parameters of cell length and stereociliary bundle side arm length (Fig. 1c) did not appear to differ along the cochlea by visual inspection and are not included in the results. However, further analysis determined that the difference in cell length was statistically significant between apex and base (Fig. 3, and Table S2a).

The distance from the IHC to OHC3 (RLW, Fig. 2a) decreased significantly from the apex to the base (W = 1066, p = <0.0001). Closest to the apex, the mean distance was 26.5 μm, while at the base the mean distance was 13.2 μm.

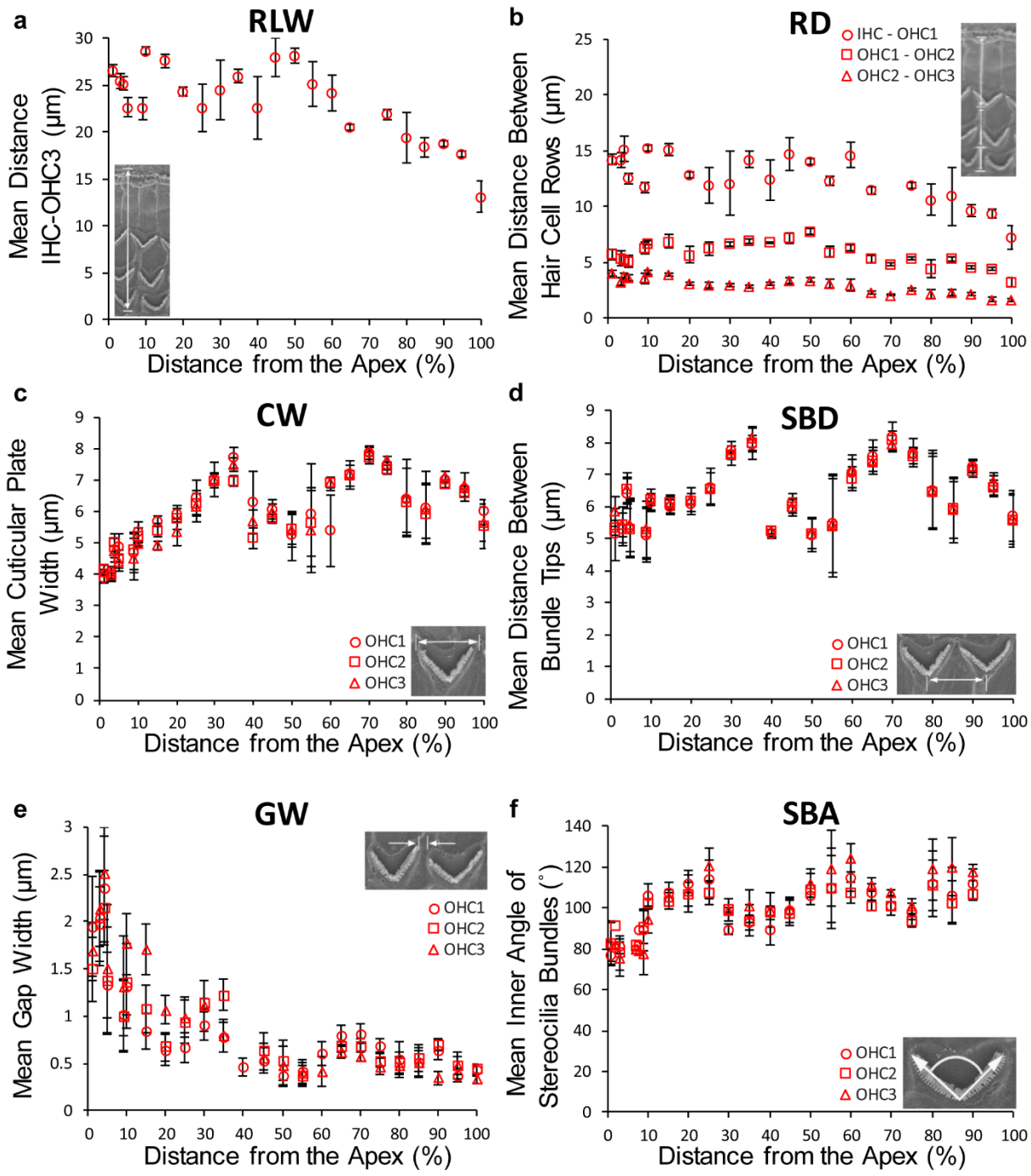

Figure 2. Six out of the eight parameters measured (Fig. 1c) that showed the greatest change from apex to base. All panels show the given parameter (mean measurement ± standard deviation) corresponding to the percent distance from the apex, along the cochlear length in Parnell's mustached bat. (n = 6). Panels (c) through (f) were measured from the outer hair cells only. (a) Parameter RLW – the distance between the inner hair cells (IHCs) to the third row of outer hair cells (OHC3) (p = <0.0001). (b)

Parameter RD – the distance between each row of hair cells (IHC - OHC1 p = <0.0001; OHC1 - OHC2 p = <0.0001; OHC2 – OHC3 p = <0.0001). (c) Parameter CW – width of the hair cell cuticular plate (CW1 p = <0.0001; CW2 p = <0.0001; CW3 p = <0.0001). (d) Parameter SBD – the distance between stereociliary bundle tips (SBD1 p = 0.5934; SBD2 p = 0.9231; SBD3 p = 0.6432). (e) Parameter GW – the gap width between stereociliary bundles (GW1 p = <0.0001; GW2 p = <0.0001; GW3 p = <0.0001). (f) Parameter SBA – the inner angle of the stereociliary bundles (SBA1 p = <0.0001; SBA2 p = <0.0001; SBA3 p = <0.0001).

Parameter RD (mean distance between rows of hair cells, Fig. 2b) decreased significantly overall from apex to base (Wilcoxon test for RD1 and RD3 and T-test for RD2). The overall decrease of these distances, along the cochlear length, was 7.0 µm (IHC-OHC1, W = 1066, p = <0.0001), 2.5 µm (OHC1-OHC2, T = 13.0814, p = <0.0001), and 2.3 µm (OHC2-OHC3, W = 1066, p = <0.0001).

Additionally, parameters CW, SBD, GW, and SBA were measured in the three rows of OHCs. For each individual parameter, the measurements among the three rows of OHCs showed a high degree of similarity, regardless of which row the hair cells were in (Figs. 2c, 2d, 2e, and 2f).

Parameter CW (OHC width, Fig. 2c) showed an overall increase from apex to base despite the fluctuations along the cochlear length. The hair cell width increased significantly in all three rows of OHCs (Wilcoxon test for CW1 and T-test for CW2 and CW3; CW1 W = 28.5, p = <0.0001; CW2 T = -6.8521, p = <0.0001; CW3 T = -9.0141, p = <0.0001).

Parameter SBD (the distance between stereociliary bundle tips, Fig. 2d), which is a measurement of the width of OHCs plus the distance between these cells among the same row, fluctuated along the cochlear length in a similar pattern to CW and SBA, although did not show a

statistically significant change between the apex and the base (Wilcoxon test; SBD1 $W = 491$, $p = 0.5934$; SBD2 $W = 525$, $p = 0.9231$; SBD3 $W = 496.5$, $p = 0.6432$).

Parameter SBA (inner angle of the OHC stereociliary bundle, Fig. 2f) showed some variability between the three rows of OHCs around 1% distance from the apex but in all three rows of OHCs increased overall from apex to base using a Wilcoxon test (SBA1 $W = 1$, $p = <0.0001$; SBA2 $W = 0$, $p = <0.0001$; SBA3 $W = 0$, $p = <0.0001$).

For CW, SBD and SBA where we did not observe a clear trend along the spiral (decreasing between 35-50%, increasing between 50-70% and decreasing beyond 70% towards the base) we performed additional statistical analyses between the region of 35-100% (Table S2b). While there were no significant differences for CW based on a Kruskal-Wallis test ($KW(2) = 5.610$, $p = 0.0605$), significant differences were found among these three regions for SBD and SBA (SBD $KW(2) = 12.9821$, $p = 0.0015$ and SBA $KW(2) = 16.5645$, $p = 0.0003$). Dunn's post-hoc test showed significant differences between 35-50% and 50-70% (SBD $p = 0.0049$; SBA $p = 0.0041$) and between 35-50% and 70-100% (SBD $p = 0.0012$; SBA $p = 0.0001$), but not between 50-70% and 70-100% (SBD $p = 0.3652$; SBA $p = 0.4709$).

The measurements of parameter GW (gap width between stereociliary bundles, Fig. 2e) showed a decreasing curve that changes more rapidly in the initial portion of the plot near the apex, and more gradually towards the base following the shape of a logarithmic curve. There was a significant difference between apex and base (GW1 $W = 1066$, $p = <0.0001$; GW2 $W = 992.5$, $p = <0.0001$; GW3 $W = 1028$, $p = <0.0001$). The mean gap widths near the apex were 1.9 µm (OHC1), 1.5 µm (OHC2), and 1.7 µm (OHC3). These gaps decreased towards the base where they were 0.4 µm (OHC1), 0.4 µm (OHC2), and 0.3 µm (OHC3). The OHC1 gap widths decreased the most, at a difference of 1.5 µm, OHC2 decreased by 1.0 µm and OHC3 decreased by 1.4 µm.

Although not included in Fig 2, CL (OHC lengths) were also analyzed (Fig. 3a). The decrease in CL in each row along the cochlear length was 0.17 µm (CL1), 0.50 µm (CL2), and 0.94 µm (CL3). All three rows of OHCs showed a significant decrease in CL between the apex and base using a T-test for CL1 and a Wilcoxon test for CL2 and CL3 (CL1 $T = 3.6631$, $p = <0.0006$; CL2 $W = 915$, $p = <0.0001$; CL3 $W = 1020$, $p = <0.0001$).

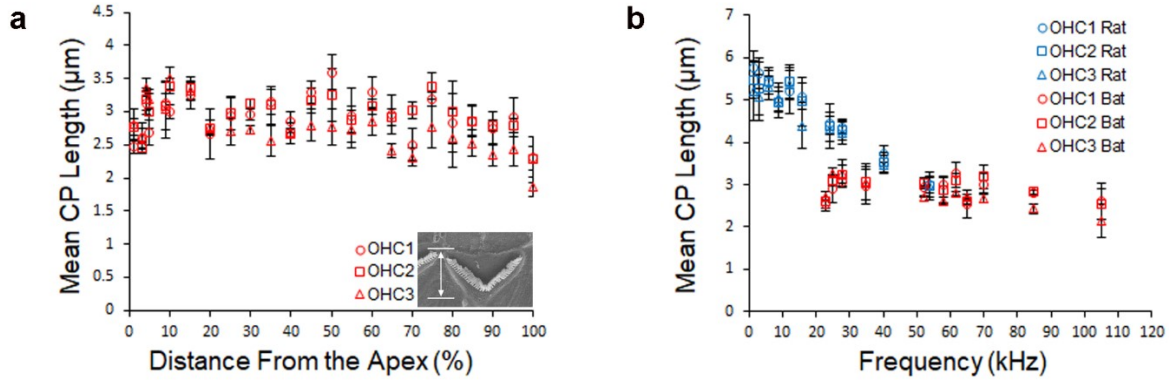

Figure. 3 Data from parameter cell length (Fig. 1c) showing the change from apex to base. Both panels show parameter cell length (CL) (mean measurement ± standard deviation) measured from the outer hair cells only. (a) Corresponding to the percent distance from the apex, along the cochlear length in Parnell's mustached bat (CL1 $p = <0.0006$; CL2 $p = <0.0001$; CL3 $p = <0.0001$) ($n = 6$). (b) These data corresponding to the frequency detected (kHz), from Parnell's mustached bat ($n = 6$) and rat ($n = 4$), for six out of the eight parameters measured (Fig. 1c) along the cochlear length plotted together.

In addition to the other morphometric parameters, the height of the stereocilia was also measured along the cochlear length of the mustached bats (Fig. 4, $n = 6$) and showed a trend similar to that seen in other echolocating bats (Yao et al. 2007). The mean stereocilia height ranged from 1.2 µm near the apex to 0.4 µm near the base, a decrease of 0.8 µm ($W = 1640$, $p = <0.0001$) (Table S2c). These stereocilia height data follow a curved path that decreases more rapidly up to a distance of 20% from the apex, after which, it changes more gradually.

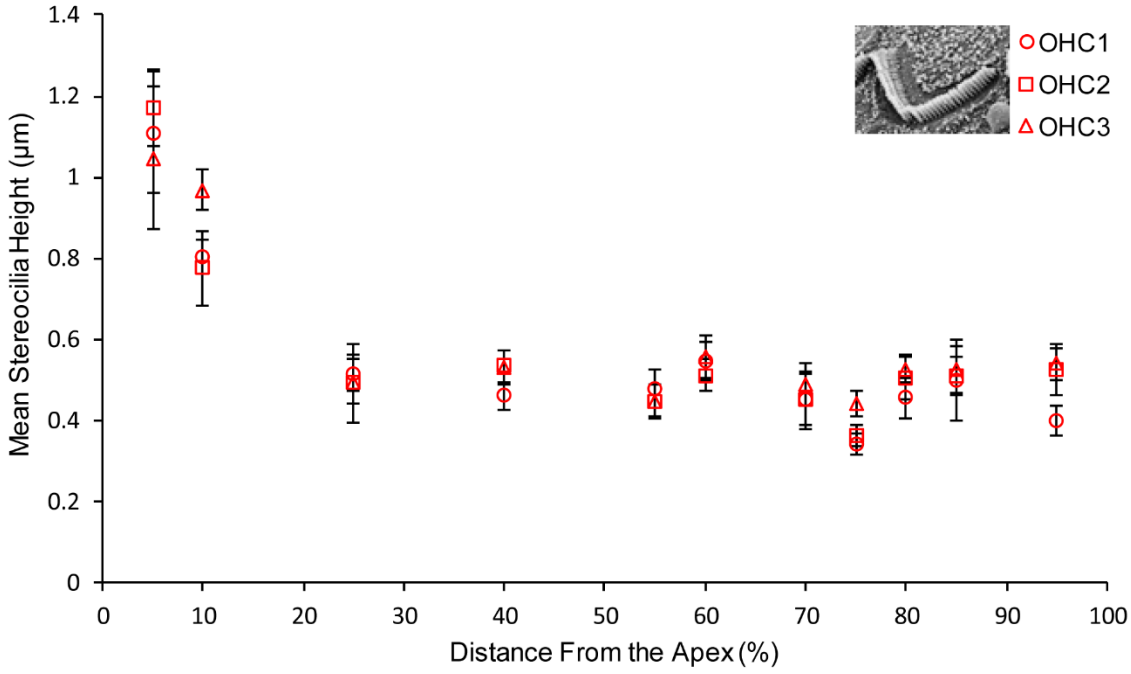

Figure 4. The mean stereocilia heights (± standard deviation) in each row of outer hair cells (OHC1, OHC2, and OHC3) in Parnell's mustached bat (n = 6). These heights were statistically different compared between the apex and the base (p = <0.0001 for all three rows).

Linear morphometric analyses of bats and rats

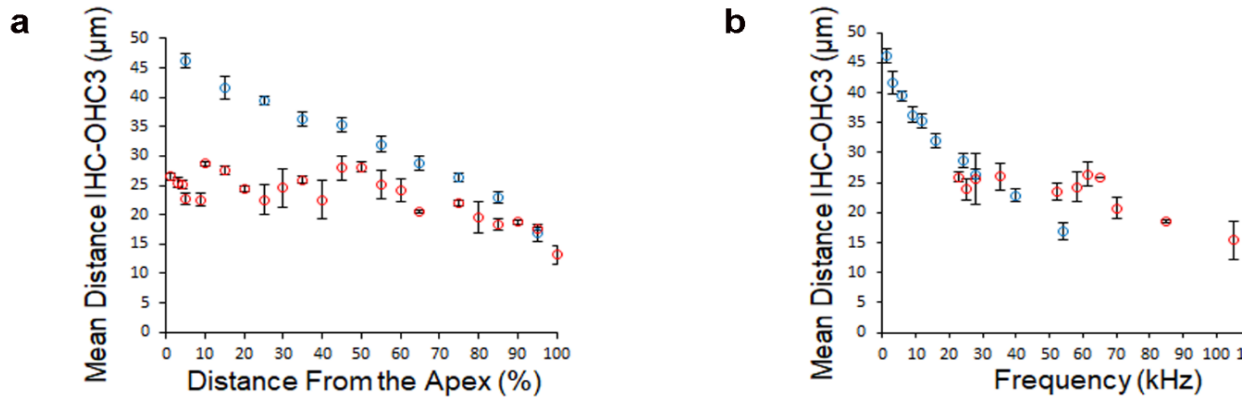

Figure 5. Data from Parnell's mustached bat (n = 6) and rat (n = 4), for one of the parameters measured along the cochlear length and plotted together versus distance (%) and again versus

frequency (kHz). The parameter shown is RLW - the distance between the inner hair cells (IHCs) to the third row of outer hair cells (OHC3) (mean measurement ± standard deviation). (a) The parameter corresponding to distance from the apex (%) along the cochlear length. (b) The same parameter corresponding to the frequency detected (kHz). In both panels the following coding is used: mustached bat (red), and rat (blue).

The mean cochlear length for four adult male rats was calculated to be 7.7 mm (± 0.3 mm). The LM measurements from the rat cochleae were taken at a distance from the apex of 5% to 95%, that corresponds to a frequency range of 1.2 to 54 kHz. Plotting the results from the bats and the rats together provides a different visual representation of the information depending on how it is plotted (Fig. 5). The parameter measurements from the two species, for example, the mean distance from IHC to OHC3 plotted together as a function of distance from the apex (%) (Fig. 5a), again showed there is a comparable change with location and that similar trends are observed in these data. However, due to the difference in hearing ranges, if these measurements are plotted as a function of frequency (Fig. 5b) we obtain a different visual representation of the information showing these data in continuity, not in parallel, and it becomes clear that the rat is a good species to use to extend the dataset to include lower frequencies. Plotting LMs from the mustached bats and rats as a function of frequency was possible because cochlear frequency maps are already available for both species (Kössl and Vater 1985, 1996; Müller 1991).

Data from the rats also showed changes in the measurements related to their location along the cochlear length (Fig. 6a – f, and Table S2d). As in the bat, the similarity between three rows of OHCs was comparable for all parameters. The measurements for the rats and bats align reasonably well to create a continuous dataset for each parameter measured, except for parameter GW (Fig. 6e), in which there was a greater variability in the hair cell morphology. There was

also a slight discrepancy between the two species in parameter CL in the region of 23 – 35 kHz (Fig. 3b).

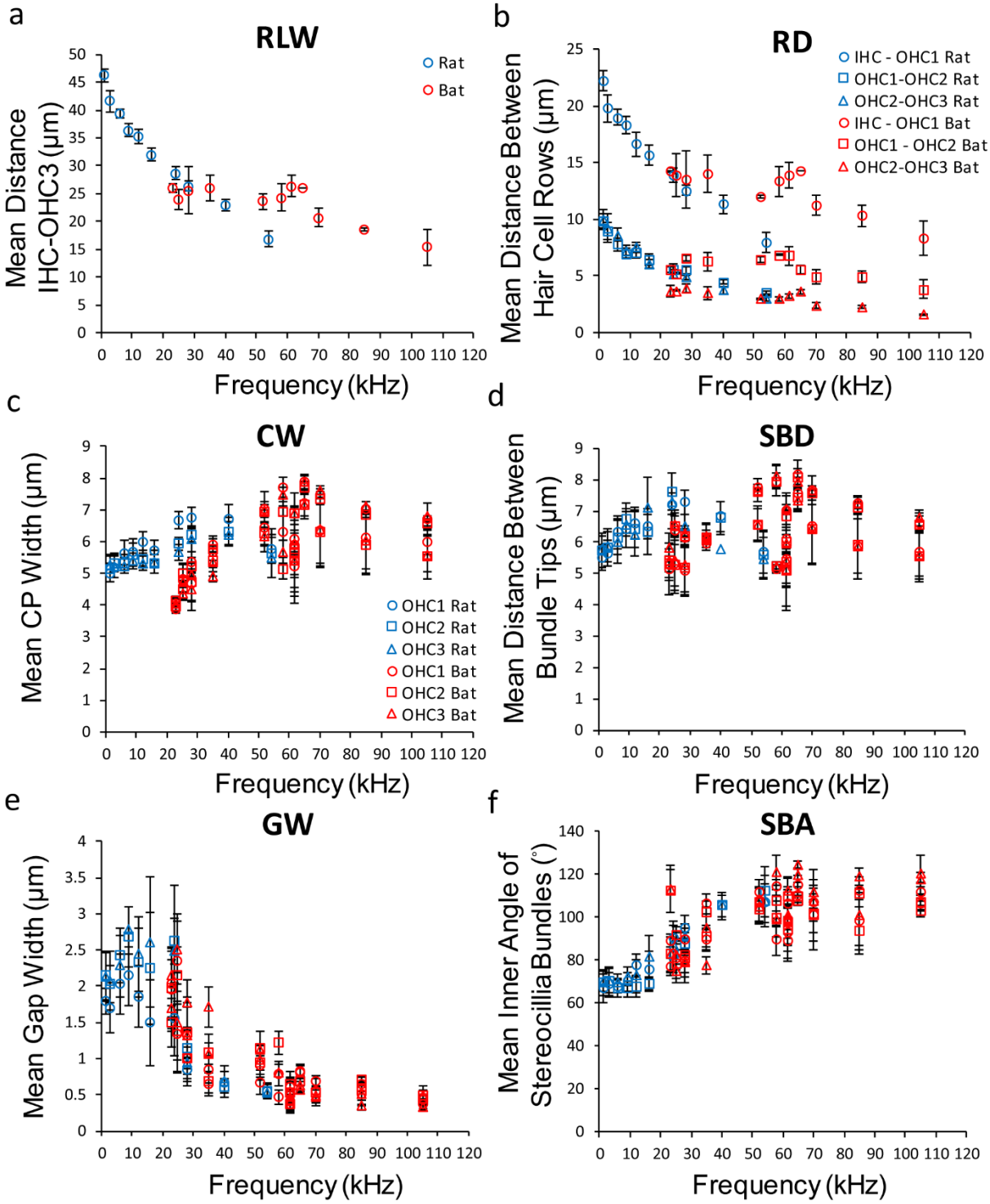

Figure 6. Data from Parnell's mustached bat (*n* = 6) and rat (*n* = 4), for six out of the eight parameters measured (Fig. 1c) along the cochlear length and plotted together. All panels show the given parameter (mean measurement ± standard deviation) corresponding to the frequency detected (kHz). Panels (c) through (f) were measured from the outer hair cells only. (a) Parameter RLW - the distance between the inner hair cells (IHCs) to the third row of outer hair cells (OHC3). (b) Parameter RD – the distance between each row of hair cells. (c) Parameter CW – width of the hair cell cuticular plate. (d) Parameter SBD – the distance between stereociliary bundle tips. (e) Parameter GW – the gap width between stereociliary bundles. (f) Parameter SBA – the inner angle of the stereociliary bundles. For Panels (d) through (f), the legend is the same as that in Panel (c).

All the LMs for bats and rats were further analyzed using statistical modelling to determine which morphological measurements were the most relevant to the frequency sensitivity. Looking first at the bat LMs, according to the AICc, 11 variables that explained the 77.4% of the variability were selected. In the bats, these variables were as follows: (RLW) the distance from IHC – OHC3, (RD1/2/3) the distance from IHC-OHC1, OHC1-OHC2, and OHC2-OHC3 respectively, (GW1/2/3) width of the gap between stereociliary bundles of OHC1s, OHC2s, and OHC3s, (CL1) cuticular plate length of OHC1s, (CW2/3) cuticular plate width from OHC2 and OHC3, and (SBA1) angle of OHC1.

Table 2. (a) Coefficients for the multiple linear regression model of the variables with the most weight calculated from the morphometrics of Parnell's mustached bat (n = 6). (b) Coefficients for the multiple linear regression model of the variables with the most weight calculated from the morphometrics of Parnell's mustached bat (n = 6) and rats (n = 4).

	Estimate	Std. Error	t value	Pr(>|t|)
(a)				
(Intercept)	110.18979	12.97791	8.491	1.34 e-15 ***
Distance IHC-OHC3 (**RLW**)	1.63798	0.6633	2.469	0.014144 *
Distance IHC-OHC1 (**RD1**)	-1.36271	0.64437	-2.115	0.035355 *
Distance OHC1-OHC2 (**RD2**)	-7.74395	1.59597	-4.852	2.06 e-06 ***
Distance OHC2-OHC3 (**RD3**)	-14.29223	2.43535	-5.869	1.27 e-08***
Gap width OHC1 (**GW1**)	-14.13181	3.25197	-4.346	1.96 e-05***
Gap width OHC2 (**GW2**)	-5.04674	2.68276	-1.881	0.061012
Gap width OHC3 (**GW3**)	-9.99442	2.43084	-4.112	5.21 e-05***
Cuticular plate length OHC1 (**CL1**)	9.4937	2.79457	3.397	0.000782 ***
Cuticular plate width OHC2 (**CW2**)	-7.24452	2.39279	-3.028	0.0027 **
Cuticular plate width OHC3 (**CW3**)	5.5813	2.24668	2.484	0.013583 *
Angle OHC1 (**SBA1**)	0.17137	0.09585	1.788	0.074904
(b)				
(Intercept)	51.04064	7.75631	6.581	1.22 e-10***
Distance IHC-OHC3 (**RLW**)	-0.70849	0.28755	-2.464	0.01409 *
Distance OHC1-OHC2 (**RD2**)	-6.15174	0.99323	-6.194	1.26 e-09***
Distance bundle tips OHC1 (**SBD1**)	-6.08962	0.99252	-6.135	1.77 e-09***
Gap width OHC3 (**GW3**)	-6.06402	1.09176	-5.554	4.60 e-08***
Cuticular plate length OHC1 (**CL1**)	8.63361	1.68415	5.126	4.28 e-07***
Cuticular plate length OHC2 (**CL2**)	4.95449	1.87251	2.646	0.00841 **
Cuticular plate length OHC3 (**CL3**)	-3.44881	1.84571	-1.869	0.06229
Cuticular plate width OHC3 (**CW3**)	4.34819	1.33442	3.258	0.0012 **
Angle OHC3 (**SBA3**)	0.45174	0.07215	6.261	8.46 e-10***
Species rat	-27.32967	2.43203	-11.237	<2.00 e-16***

Number of stars indicates the weight of each variable in explaining the frequency.
Significance codes: 0 '***' / 0.001 '**' / 0.01 '*' / 0.05 '.' / 0.1 ' ' / 1

The results of rat LMs found to be the most significant explain 98.1% of the variation related to frequency sensitivity according to the AICc. The 12 selected variables are the

following: (RLW) distance from IHC-OHC3, (RD3) the distance OHC2-OHC3, (GW2/3) width of the gap between stereociliary bundles of OHC2s, and OHC3s, (CL1/2) cuticular plate length of OHC1s and OHC2s, (CW3) cuticular plate width from OHC3, (SBD1/3) distance between the stereociliary bundle tips of OHC1s and OHC3s, and (SBA1/2/3) the inner angle of the stereociliary bundles of OHC1, OHC2 and OHC3.

Combining the LM measurements from the bats and rats, we used the AICc criteria to select the most significant variables (Table 2b). The nine variables selected when combining the data from rat and bat are: RLW, RD2, SBD1, GW3, CL1/2/3, CW3 and SBA3 (Fig. 7), which explain 86.9% of the variation related to frequency sensitivity.

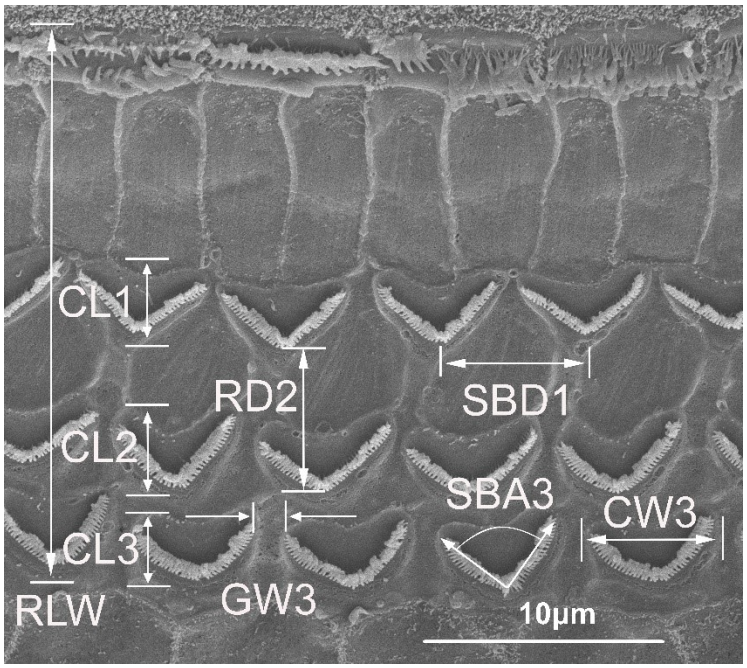

Figure 7. The parameters that explained the majority of the variation. The nine variables that explained 86.9% of the variation related to frequency sensitivity combining the data from Parnell's mustached bat (n = 6) and rats (n = 4).

We could calculate the predicted frequencies along the cochlear spiral for a given species based on the results of the multiple linear regression model (Table 2b), and the LMs from the mustached bats and rats, using the following equation:

$$Estimated\ Frequency\ (kHz) = 51.041 - (SBA3 \times 0.45) - (SBD1 \times 6.09) - (GW3 \times 6.06) - (RLW \times 0.71) + (CL1 \times 8.63) - (RD2 \times 6.15) + (CL2 \times 4.95) - (CL3 \times 3.45) + (CW3 \times 4.35) - (Species\ Rat \times 27.32)$$

The error in the prediction is $(51.04 \pm 7.76) - (SBA3 \times (0.45 \pm 0.07)) - (SBD1 \times (6.09 \pm 0.99)) - (GW3 \times (6.06 \pm 1.09)) - (RLW \times (0.71 \pm 0.29)) + (CL1 \times (8.63 \pm 1.68)) - (RD2 \times (6.15 \pm 0.99)) + (CL2 \times (4.95 \pm 1.87)) - (CL3 \times (3.45 \pm 1.85)) + (CW3 \times (4.35 \pm 1.33)) - (Species\ Rat \times (27.32 \pm 2.43))$.

Since the measurements for each parameter vary with location along the cochlear length, entering the value of each of the nine parameters at each cochlear position into this equation gives us the frequency for a given location. In addition to the parameters, this equation also contains a coefficient (Species Rat) that is used to balance the equation when more than one species is combined with a different hearing frequency range to create a model such as this one. The value *Species Rat* is = 1 if the data is from a rat and = 0 if the data is from a bat. Repeating this for locations along the entire cochlear length generates a complete set of values for frequency as a function of location, or the frequency map.

Geometric morphometric analysis in Parnell's mustached bat

As seen by the placement of the landmarks in Fig. 1d, there is variation in the hair cell shape, particularly in the OHCs from apex to base along the organ of Corti. This variation does not change regularly along the entire cochlear length, although it does change overall from apex

to base (Fig. 8). Closest to the apex of the cochlea, the individual OHCs are more compact, with a larger gap width between them as a result (Fig. 8a). Moving along the cochlear length, the width of the OHCs increases and the associated gap width decreases (Fig. 8b). The OHC length also decreases making the cells appear more flattened. Near the base of the cochlea, the hair cells are wider and flatter still and consequently the gap width is further reduced (Fig. 8c). The spacing between rows is also greater in the apex region (Fig. 8a) and decreases along the cochlear length to the base, where the row spacing is reduced (Fig. 8c).

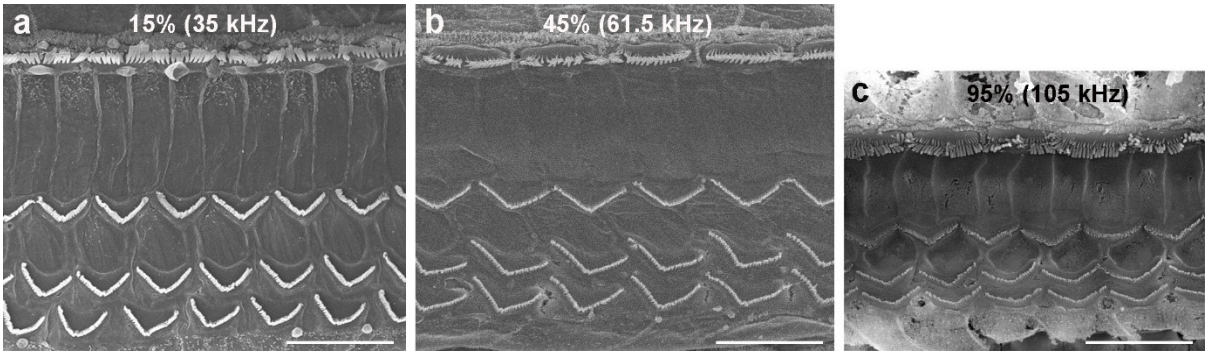

Figure 8. The variation in hair cells. Scanning electron micrographs from three of the ten locations (showing hair cells from 15, 45 and 95% distance from the apex) for which geometric morphometrics were analyzed along the organ of Corti of Parnell's mustached bat. Frequencies were extracted from the cochlear frequency map of the mustached bat (Kössl and Vater 1985). Scale bars = 10 μm.

The Principal Component Analysis (PCA) performed on blocks of 12 cells (3 IHCs and 9 OHCs, Fig. 9) showed in this case that PC1 was responsible for 59.5% of the variation (eigenvalue of 0.01196996), and PC2 was responsible for 21% of the variation (eigenvalue of 0.00429978). It is difficult to see a clear pattern in these data relating changes in cell shape to the location along the organ of Corti.

The PCA performed on individual cells grouped by IHCs and OHCs (Fig. 9b) showed that the variation in cell shape as a function of location along the cochlear length differed

between the IHCs and OHCs. However, the variation due to PC1 was particularly high at 74%, with only 20% attributable to PC2. In this case, the shape changes associated with the IHCs are visible in a cluster on the left-hand side of the panel and the locations are interspersed throughout, indicating little variation in shape associated with location. In the OHCs there was a more distinct relationship between the variation in cell shape related to location along the cochlear length, represented on the right-hand side of Fig. 9b. The shape change of the OHCs is indicated by a more widely dispersed grouping of data points in which there is a differentiation of the cells with respect to their location along the cochlea.

Performing the PCA only on individual OHCs (Fig. 9c) revealed that PC1 was responsible for 56% of the variation, and PC2 for 29% of the variation. The relationship between the change in hair cell shape due to both PC1 and PC2, and location along the organ of Corti is clearly visible in this analysis of the OHCs. This also reflects the morphological changes in the hair cells independently from their relationship to other hair cells, either in the same or neighbouring rows. From apex to base along the cochlear length, changes in both IHCs vs OHCs, as well as for only OHCs, the first four PCs were responsible for a total of 100% of the hair cell shape variation. When comparing the first PC with the coding frequency, we observed a clear trend along the spiral (Fig. 10a). The regression between hair cell shape (Procrustes) and frequency (Fig. 10b) showed variation in shape (calculated as the deviation from the mean shape) related to frequency and location. The overall shape of the OHCs varied in several interconnected ways along the cochlear length. For instance, the inner angle of the stereocilia of the OHCs became larger with increasing distance from the apex, resulting in shallower v-shaped bundles at the base of the cochlea. Related to this change was an increase in the width of the OHCs and a resultant flattened appearance to the cells due to a decrease in the cell height, again moving along the cochlear length from apex to base.

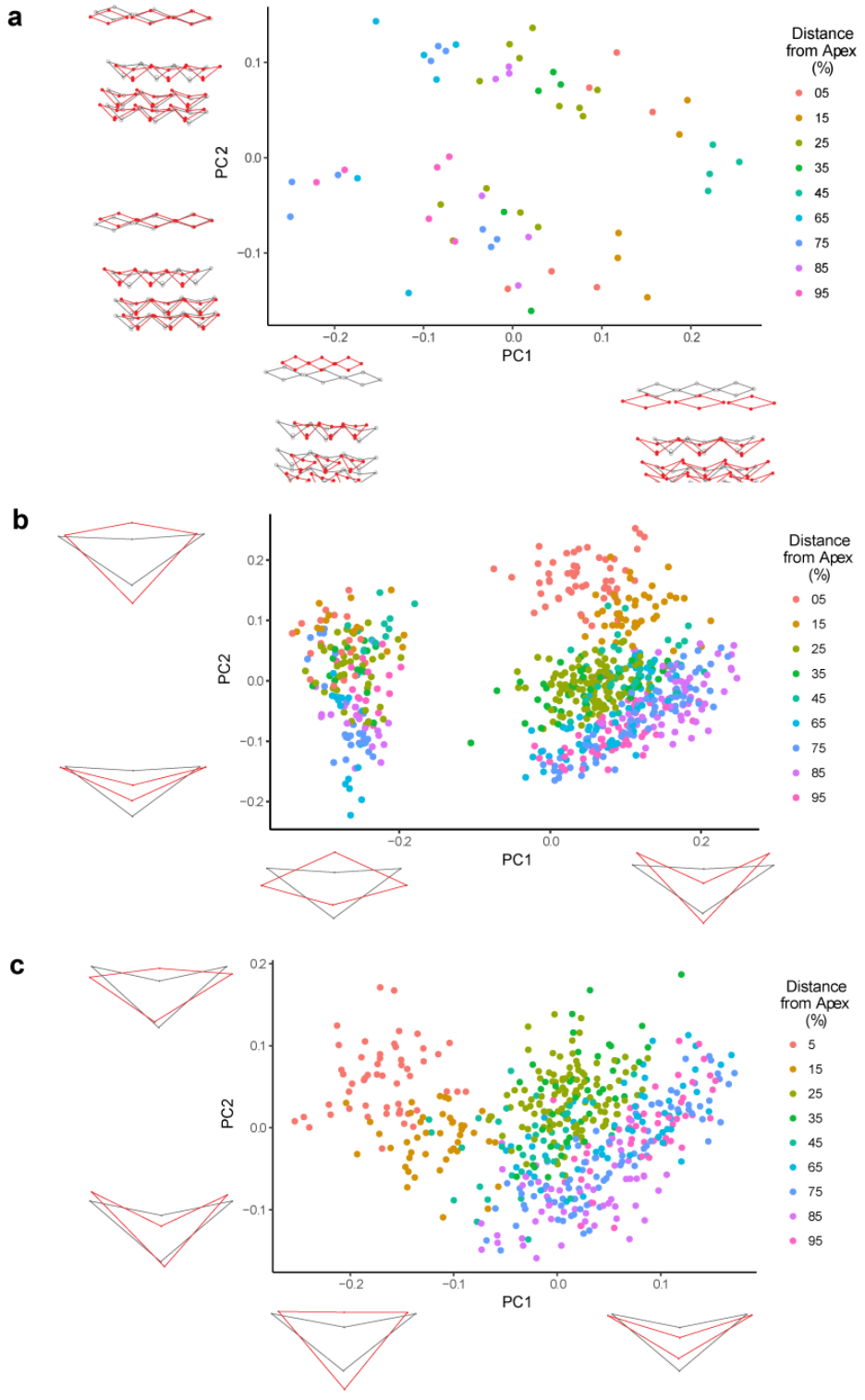

Figure 9. **Principal component analysis (PCA) results from the geometric morphometric measurements of Parnell's mustached bat.** (a) Analysis of the blocks of inner hair cells (IHCs) and outer hair cells (OHCs) analyzed together as a block of twelve cells in total (3 IHCs and 9 OHCs). (b)

Analysis of the inner hair cells separated from and compared to the outer hair cells. (c) Analysis of only the outer hair cells (n = 6). Wireframes adjacent to the axes in all panels represent the shape changes of the hair cells. The grey shapes represent the average shape after the Procrustes fit (i.e. due to position, orientation and scale removed), while the red shapes represent the average shape of the hair cells due to each principal component.

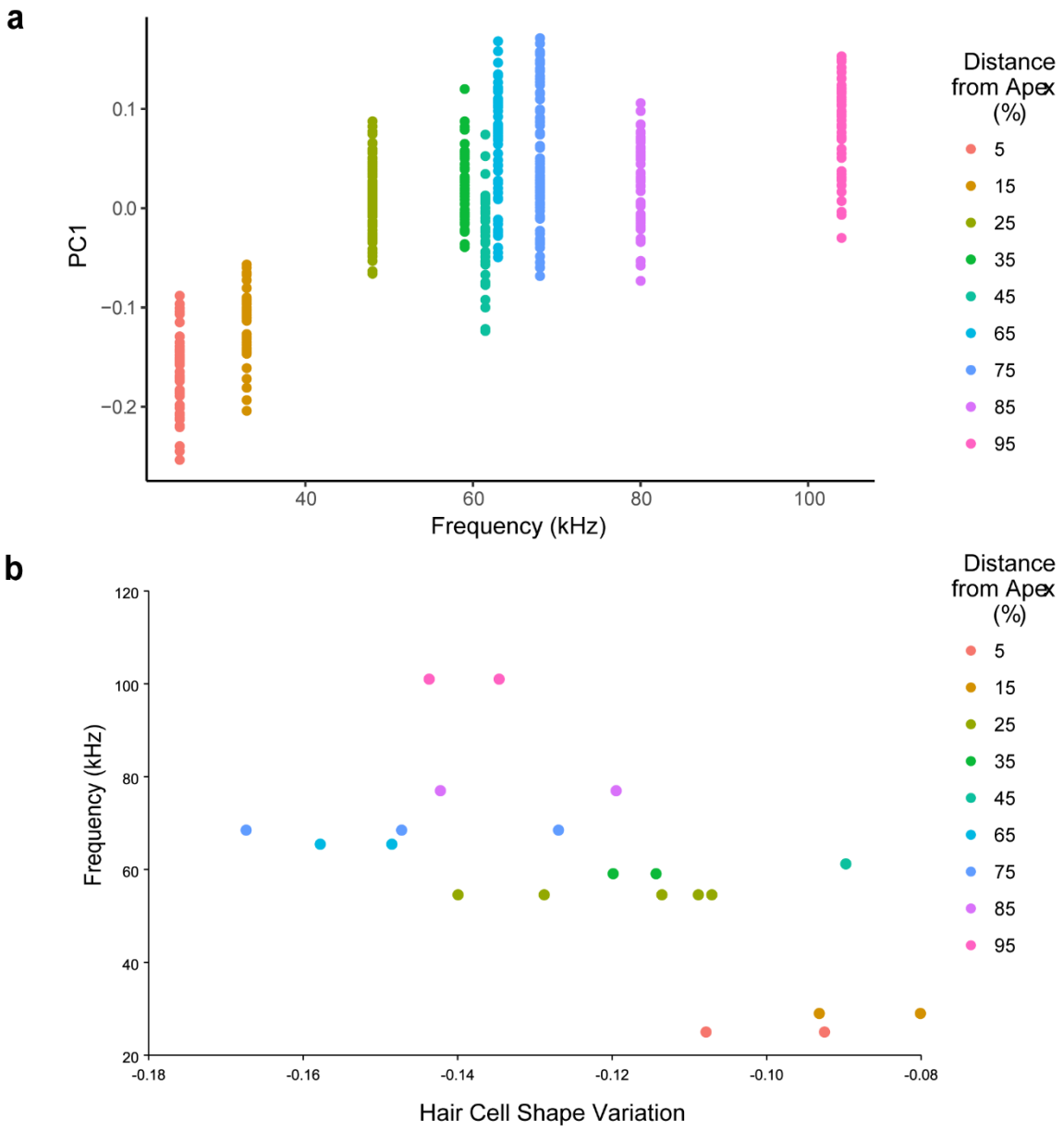

Figure 10. Principal component one as a function of frequency (kHz), and a linear regression of frequency versus variation in hair cell shape using geometric morphometric measurements from

Parnell's mustached bat. (a) Principal component one (PC1) as a function of frequency showing the variation in outer hair cell shape corresponding to locations from 5 – 95% distance from the apex. (b) Regression results of frequency versus inner and outer hair cell shape (Procrustes), averaged by individual and location (% distance from the apex) (n = 6).

Geometric morphometric analysis in the Wistar rat

Using the same landmark placement as in the bats (Fig. 1d), similar variation was observed in the hair cell shape, particularly in the OHCs, from apex to base along the organ of Corti. The variation and trends in cell shape and spacing seen in the hair cells of the bats (Fig. 8) was comparable to the variation seen in the rats.

The Principal Component Analysis (PCA) performed on blocks of 12 cells (3 IHCs and 9 OHCs, Fig. 11a) showed in this case that PC1 was responsible for 55% of the variation (eigenvalue of 0.02325598), and PC2 was responsible for 22.8% of the variation (eigenvalue of 0.00962291). Compared to bats, the rat data exhibited a more defined separation into two groups and a clearer pattern relating the changes in the cell shapes to the location along the organ of Corti.

Similar to our observations in the bat, PCA performed on individual cells grouped by IHCs and OHCs (Fig. 11b) showed that the variation in cell shape occurred as a function of location along the cochlear length, and differs between the IHCs and OHCs. However, the variation was again primarily due to only two PCs; PC1 being 68.4% and PC2 being 25%. In this case, the shape changes associated with the IHCs are visible in a cluster on the top left-hand side of the panel and the locations are again, interspersed throughout and indicative of little variation in shape associated with location. In the OHCs there was a more distinct relationship between the variation in cell shape related to location along the cochlear length, represented on the lower

right-hand side of Fig. 11b. The shape change of the OHCs is visually represented by a wider dispersal of these data points in which there is a visible differentiation of the cells with respect to their location along the cochlea.

The PCA on only the individual OHCs (Fig. 11c) revealed more than 90% of the total variation was in PC1 (75%) and PC2 (15.5%). The relationship between the change in hair cell shape due to both PC1 and PC2, and location along the organ of Corti was once again clearly visible in this analysis of the OHCs. This also depicts the morphological changes in these hair cells independently from their relationship to other hair cells, either in the same or neighboring rows. As previously seen in the bat analyses, here in the rats, the first four PCs were also responsible for a total of 100% of the hair cell shape variation from apex to base along the cochlear length with regards to the changes in both the analysis of IHCs vs OHCs, as well as for the isolated OHCs. The overall shape of the OHCs varied in several interconnected ways along the cochlear length including the inner angle of the stereocilia of the OHCs that became larger with increasing distance from the apex, resulting in shallower v-shaped bundles at the base of the cochlea. Associated with this change was a subsequent increase in the width of the OHCs and, as a result, a flattened appearance due to a decrease in cell height, again moving along the cochlear length from apex to base.

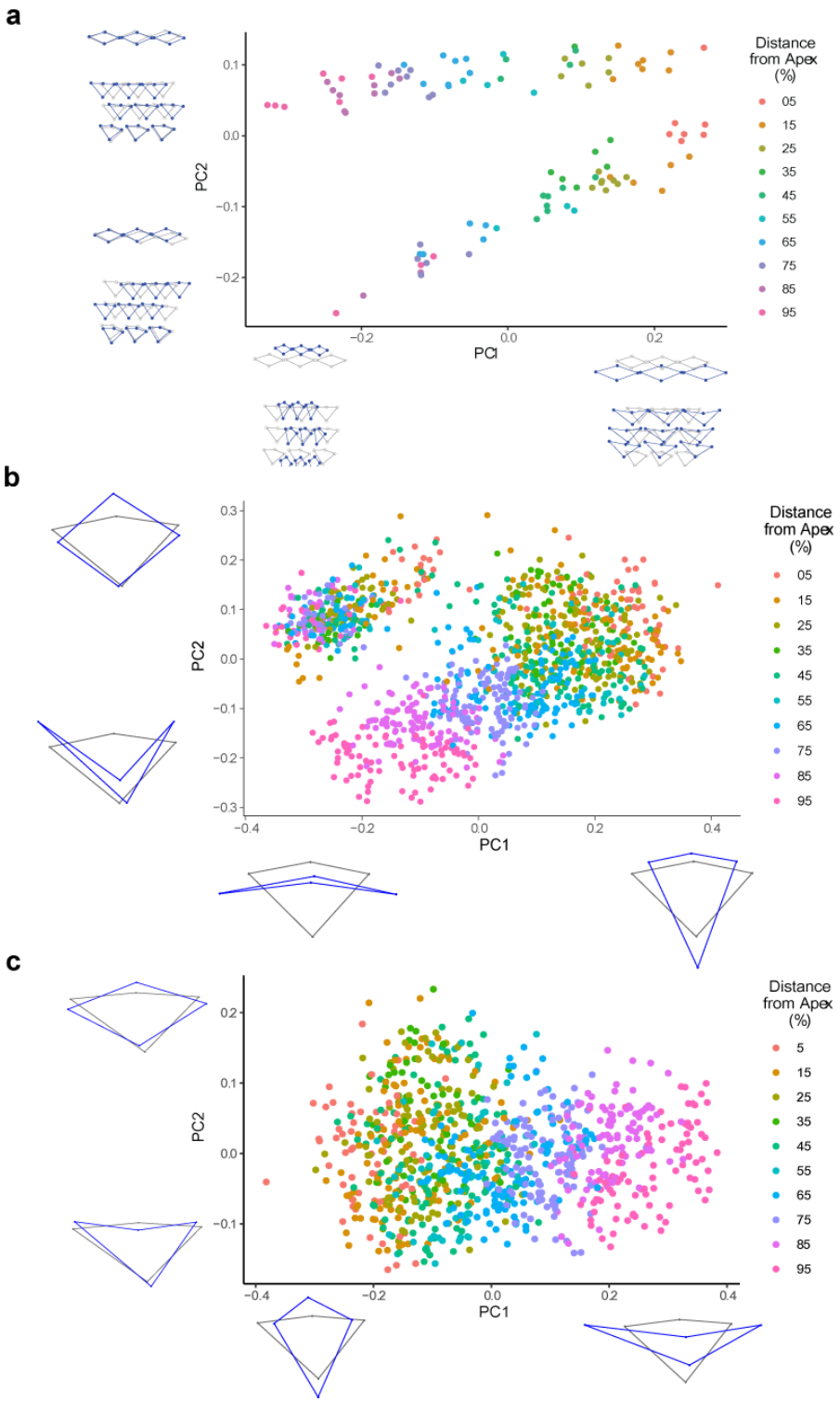

Figure 11. Principal component analysis (PCA) results from the geometric morphometric measurements from the rat. (a) Analysis of the blocks of inner hair cells (IHCs) and outer hair cells (OHCs) analyzed together as a block of twelve cells in total (3 IHCs and 9 OHCs). (b) Analysis of the

inner hair cells separated from and compared to the outer hair cells. (c) Analysis of only the outer hair cells (n = 4). Wireframes adjacent to the axes in all panels represent the shape changes of the hair cells. The grey shapes represent the average shape after the Procrustes fit (i.e. due to position, orientation and scale removed), while the blue shapes represent the average shape of the hair cells due to each principal component.

GM analyses of hair cells in the bat and rat cochleae provide information about the variation in cell shape, as a function of the location along the cochlear length. This supplements the information from LM regarding the spacing of the hair cells, as well as linear components of the hair cell morphometrics that contribute to their shape and strengthens our understanding of the overall changes in the shape of the hair cells.

Discussion

Linear morphometric analysis

The average value of the cochlear length for mustached bat measured in our study (10.53 mm) is smaller than previously published for the species (average of 14.3 mm, Kössl and Vater 1985). The disparity could be due to different origins of the samples (Jamaican *versus* Cuban population in our study), or differences in the processing technique (flat preparations under light microscopy *versus* SEM here). A direct attribution of certain anatomical cochlear parameter variations to body size was not possible due to the small number of samples. The cochlear samples we analyzed possessed two and a half cochlear turns, which corresponds with previous findings (Kössl and Vater 1985).

The results for the width of the reticular lamina (RLW) (Fig. 1c, Fig. 2a) and row distance (RD) (Fig. 2b) in mustached bats showed a decrease from apex to base. These two

parameters changed together as expected and as reported previously in other mammals (Dallos 1992; Lim 1986).

In the bat, parameters (Fig. 1c): cell width (CW) (Fig. 2c), gap width (GW) (Fig. 2e), stereociliary bundle inner angle (SBA) (Fig. 2f), and cell length (CL) showed significant overall changes.

We expected to find little variation in the morphometrics of the cuticular plate of the organ of Corti in the region of the auditory fovea (located between 40 and 60% of the cochlear length) since this is a region in mustached bats that is specifically tuned to 61.5 kHz ((Kössl 1994b), the biologically important frequency for their echolocation (Kössl and Vater 1985). Morphological parameters that are relevant for frequency representation and tuning should not change significantly across the fovea, such as the basilar membrane width and thickness/width ratio. Still, some parameters in this region (CW and SBD) had more variability than others (RD, GW), although the relevance of this finding is not clear. The fact that some parameters vary within the auditory fovea could mean that 1) either they do not play an important role for frequency representation, and therefore variations are evolutionarily tolerated, 2) some parameters contribute more to frequency selectivity, 3) the results obtained could be due to inter-individual variability and/or 4) there are other constraints besides frequency representation that are relevant for these parameters (CW, SBD). The nine parameters that describe the maximum variability, according to the predictive model presented here, are also those that change the least in the auditory fovea, except for CW3.

SBA (Fig. 2f) showed some variability between the three rows of OHCs around 1% distance from the apex but increased overall from apex to base. As expected from previous studies (Vater and Lenoir 1992; Vater and Siefer 1995) the mean inner angle increased for OHC1 from apex to base. Surprisingly, these angles decreased in OHC2 and OHC3, as the apical

values were from a single bat. OHC1 looked typical for cells close to the apex. However, those from OHC2 and OHC3 were flatter and wider, similar to hair cells closer to the base, possibly due to the angle at which the picture was taken. Removing this single location from the one individual from the dataset results in a shift to where the mean inner angle increases from apex to base, as in other mammals. Processing of the cochlear samples for SEM imaging may be implicated in the variation found in the apex, as tissue shrinkage due to fixation and critical point drying likely occurs, but previous work has shown that the variability due to processing should be consistent among samples and locations of the cochlea processed using the same methodology (Edge et al. 1998; Yarin et al. 2014).

The decrease in OHC stereocilia heights in the mustached bat from apex to base followed a descending curve that changed most rapidly from 0 to 20% distance from the apex (Fig. 4). This pattern was also seen in four other species of echolocating bats with OHC stereociliary heights similar to the mustached bats analyzed here (Yao et al. 2007). However, the frequencies that are represented in the apical 20% in the study of Yao and colleagues could probably be different than in mustached bats. The OHC stereocilia of echolocating bats have also been found to be shorter than those of non-echolocating mammals and vary tonotopically along the cochlear length (Dannhof and Bruns 1991; Vater and Lenoir 1992; Vater and Siefer 1995; Vater and Kössl 1996). Our findings provide further morphological evidence to support previous studies stating that the small size of stereocilia in echolocating bats may be likely related to the ability to process high frequency sounds (Vater and Lenoir 1992), since the resonance frequency of the stereociliary bundle is inversely related to the bundle height (Wright 1984; Strelioff et al. 1985).

There were several parameters (CW, SBD, GW, and SBA, Fig. 1c) that had lower values for the basal-most data point (at 99.65% distance), relative to the previous data points in each set. It is not clear why this is the case, but our results are consistent with previous work where other

researchers have found the same contrary tendency in the basilar membrane within the first micrometers of the base, known as the hook (for its shape), in echolocating whales and bats (Bruns 1976; Dannhof and Bruns 1991; Kössl and Vater 1985; Morell et al. 2015). In addition, it is difficult to image the hook effectively for analysis using morphometric measurements, as well as for other types of studies (Rhode and Recio 2000). Further modelling and measurements would help give further insight to this trend, although this is beyond the scope of this study.

To predict a cochlear frequency map from LM measurements for species with hearing ranges that extend below that of Parnell's mustached bat we included data from another mammal, in this case the rat. When plotted as a function of distance from the apex (Fig. 5a) the bat and rat data sets for the parameter RLW were distinctly different but, when plotted as a function of frequency, these data converged across their common frequencies, resulting in a relatively continuous relationship that extended from 1.2 to 112 kHz (Fig. 5b). We subsequently did this for all the LM parameters (Fig. 6) and found that bat and rat data generally align well, giving a complete range of LM measurements linked to the frequencies encoded by these hair cells. The LM measurements for the bats and rats required further analysis to determine which of the parameters, and from which OHC row, were the most relevant for predicting a cochlear frequency map. Each parameter consists of measurements from all three rows of OHC and may, therefore, contain variations.

Using statistical modelling and combining the parameters that explained the majority of the variance in the mustached bats with parameters from the rats, the selection of models based on AICc criterion took the nine variables that explained 86.9% of the variance related to frequency selectivity, and a multiple linear regression model was created (Table 2b). The variables for mustached bats and rats were: RLW, RD2, SBD1, GW3, CL1/2/3, CW3 and SBA3. Further research that includes other species with known frequency maps in the predictive model,

will give us a better insight on the range and/or variability of species coefficients. Once the predictive value of our model is validated with other model species, the resultant equation could potentially be used to calculate a frequency map for additional mammalian species, for which physiological methods of creating frequency maps are not feasible, for example, echolocating whales. In this instance, species of whales with known audiograms will be crucial for adjusting the coefficients, since we will be able to adjust the results of the predicted frequency maps with the frequency range of hearing measured with the species audiograms. The ability to use morphological measurements supported by auditory information is essential in validating the creation of cochlear frequency maps from LM measurements and morphological structures common among mammalian species.

Geometric morphometric analysis

LM analysis is informative but limited to linear measurements. For information of cell shape and how it varies along the cochlea, which could also be relevant, we applied the GM method. This considers interactions among selected landmark coordinates and removes variation other than that related to the shape. To our knowledge, this is the first study to examine the variation in hair cell cuticular plate shape along the cochlear length using GM analysis.

While analyzing all these data together did not show any clear pattern with respect to the first PCs (Fig. 9a), the OHCs were separated from IHCs (Fig. 9b) and the OHC shape was clearly defined among locations (Fig. 9c) when data were separated in two blocks: IHCs and OHCs. This analysis indicated that shape variation in OHCs is linked to location and its corresponding frequency, with a particularly high amount of the variation attributed to only two PCs. This variation of the OHCs is visualized in wireframe shapes seen along the axes in Fig. 9. These two PCs also related to the LM measurements that, in combination, resulted in the overall hair cell

shape. For example, a widening and flattening of the shape results from an increase in the width of a hair cell and a decrease in cell length, as well as an increase in the inner angle of the stereociliary bundles. Associated with the increase in width and overall shape change was also a decrease in the gap width between cells. As in the LM analysis, it would seem that PC1 and PC2 relate in varying degrees to the cell length, cell width, inner angle of the stereociliary bundles, and gap width. Additionally, when looking at the analysis of IHCs and OHCs combined (Fig. 9a) PC1 and PC2 relate to the spacing between the cell rows.

In Figure 10a the clear separation of the data points links the change in hair cell shape from apex to base, and therefore morphometrics, with both frequency and location. This further supports the findings from the LM analysis. The similarity of hair cell shape in the mid-region of the cochlea, and related to the acoustic fovea, may require further analysis to determine differences in the shape of the hair cells in this region that may be subtler, if present at all.

A regression of the hair cells in the bats also showed a relationship between hair cell shape and frequency (Fig. 10b). The overall shape of the OHCs varied from the apex to the base along the cochlear length, a consequence of variation in the individual LM parameters comprising the shape. The OHC shape became wider and flatter towards the base. This is a product of an increase in the inner angle of the stereociliary bundles that, in turn, corresponds to shallower v-shaped bundles at the base of the cochlea.

Geometric morphometric analysis in rats gave comparable results as in mustached bats (Fig. 11). The presence of the relationship between shape and frequency in both the bats and rats, further indicates that shape can be used to understand more about the morphometrics of hearing in general, across species, as well as having the potential to help fine-tune mammalian frequency maps.

The tonotopic organization of the organ of Corti has been well documented (Müller et al. 2005; Dallos 1992; Kössl and Vater 1990a, 1990b). Our results from both LM and GM analyses show a strong relationship between the frequencies detected and the location along the cochlear length at which they are detected. Studying an echolocating mammal, supplemented with measurements from the rat, has shown how the morphological features of the cuticular plate of the organ of Corti depend on and/or define frequency representation. Micromorphological parameters that depend on cell size and structure will yield additional information that could inform models (finite element, analytical, fluid dynamic) designed to explore the physics of cochlear tuning mechanisms. Specifically, our study shows that the higher variability and association with encoding frequency relies on the morphometrics of the cuticular plate from OHCs that are essential for frequency selectivity.

Further linking frequency sensitivity with morphological variation in sensory hair cells is of increasing importance, given our need to understand how anthropogenic noise is impacting mammals, particularly cetaceans. In species for which standard frequency mapping techniques and developing audiograms are difficult at best and often not feasible at all, connecting morphology to encoding frequency can provide alternative techniques to better understand hearing. For such species, most often marine mammals, creating a prediction of their frequency map yields a way to determine the encoding frequency of lesions in the cochlea as a result of noise-induced hearing loss. In addition, our data will be crucial for modelling studies of energy flow in the sub-tectorial space. Determining this biologically relevant process in relation to frequency detection can give us a greater understanding of the essential biomechanical characteristics for frequency selectivity during sound transduction.

Acknowledgements

The authors thank Christina Harvey for help with R and geomorph, Vikram Baliga for helping with the geomorph coding that he and C.H. developed. We also thank Derrick Horne (UBC Bioimaging Facility) and Dr. Chantal Cazevieille (COMET) for technical assistance, and Dr. Marc Lenoir (Institute for Neurosciences of Montpellier) for dissecting and processing the rat cochleae. Funding for the research described herein was provided by the Natural Sciences and Engineering Research Council of Canada (NSERC) (RGPIN 312039-13 and RGPAS 446012-13 to R.E.S.) and the Department of Zoology at the University of British Columbia. The research leading to these results has also received funding from Marie Skłodowska-Curie Individual Post-doctoral Fellowship 751284-H2020-MSCA-IF-2016 to M.M.

Competing interests

The authors declare that they have no conflict of interest.

This is a post-peer-review, pre-copyedit version of an article published in Journal of the Association for Research in Otolaryngology. The final authenticated version is available online at: http://dx.doi.org/10.1007/s10162-020-00764-1

References

Adams DC, Collyer ML, Kaliontzopoulou A (2018) Geomorph: Software for geometric morphometric analyses. R package version 3.0.6

Barton K (2019) Multi-modal inference - R Package 'MuMIn.' R Packag. version 1

Bruns V (1976) Peripheral auditory tuning for fine frequency analysis by the CF-FM bat, *Rhinolophus ferrumequinum* - I. Mechanical specializations of the cochlea. J Comp Physiol A 106:77–86. doi: 10.1007/BF00606573

Burnhan KP, Anderson DR (2002) Model selection and multimodel inference. New York Springer

Ciganović N, Wolde-Kidan A, Reichenbach T (2017) Hair bundles of cochlear outer hair cells are shaped to minimize their fluid-dynamic resistance. Sci Rep 7:1–9. doi: 10.1038/s41598-017-03773-y

Dallos P (1992) The active cochlea. J Neurosci 12:4575–4585

Dannhof BJ, Bruns V (1991) The organ of Corti in the bat *Hipposideros bicolor*. Hear Res 53:253–268

Dannhof BJ, Roth B, Bruns V (1991) Length of hair cells as a measure of frequency representation in the mammalian inner ear? Naturwissenschaften 78:570–3. doi: 10.1007/BF01134454

Echteler SM, Fay RR, Popper AN (1994) Structure of the mammalian cochlea. In: Fay RR, Popper AN (eds) Comparative hearing: Mammals. Springer, New York, NY, pp 134–171

Edge RM, Evans BN, Pearce M, et al (1998) Morphology of the unfixed cochlea. Hear Res 124:1–16

El Naqa I, Murphy MJ (2015) What is machine learning? In: El Naqa I, Li R, Murphy MJ (eds) Machine Learning in Radiation Oncology: Theory and Applications. Springer International Publishing, Cham, pp 3–11

Fettiplace R, Kim KX (2014) The physiology of mechanoelectrical transduction channels in hearing. Physiol Rev 94:951–986. doi: 10.1152/physrev.00038.2013

Guinan JJ (2012) How are inner hair cells stimulated ? Evidence for multiple mechanical drives. Hear Res 292:35–50. doi: 10.1016/j.heares.2012.08.005

Jolliffe IT (2002) Principal component analysis, Springer series in statistics, 2nd edn. Springer-Verlag New York, New York

Klingenberg CP (2011) MorphoJ: An integrated software package for geometric morphometrics. Mol Ecol Resour 11:353–357. doi: 10.1111/j.1755-0998.2010.02924.x

Kössl M (1994a) Evidence for a mechanical filter in the cochlea of the "constant frequency" bats, *Rhinolophus rouxi* and *Pteronotus parnellii*. Hear Res 72:73–80. doi: 10.1016/0378-5955(94)90207-0

Kössl M (1994b) Otoacoustic emissions from the cochlea of the 'constant frequency' bats, *Pteronotus parnellii* and *Rhinolophus rouxi*. Hear Res 72:59–72. doi: 10.1016/0378-5955(94)90206-2

Kössl M, Vater M (1985) The cochlear frequency map of the mustache bat, *Pteronotus parnellii*. J Comp Physiol A 157:687–697. doi: 10.1007/BF01351362

Kössl M, Vater M (1996) Further studies on the mechanics of the cochlear partition in the mustached bat. II. A second cochlear frequency map derived from acoustic distortion products. Hear Res 94:78–86. doi: 10.1016/0378-5955(96)00006-8

Kössl M, Vater M (1990a) Tonotopic organization of the cochlear nucleus of the mustache bat, *Pteronotus parnellii*. J Comp Physiol A 166:695–709. doi: 10.1007/BF00240019

Kössl M, Vater M (1990b) Resonance phenomena in the cochlea of the mustache bat and their contribution to neuronal response characteristics in the cochlear nucleus. J Comp Physiol A 166:711–720. doi: 10.1007/BF00240020

Lim DJ (1986) Functional structure of the organ of Corti: a review. Hear Res 22:117–146. doi: 10.1016/0378-5955(86)90089-4

Lim KM, Steele CR (2002) A three-dimensional nonlinear active cochlear model analyzed by the WKB-numeric method. Hear Res 170:190–205. doi: 10.1016/S0378-5955(02)00491-4

Morell M, Brownlow A, McGovern B, et al (2017) Implementation of a method to visualize noise-induced hearing loss in mass stranded cetaceans. Sci Rep 7:41848. doi: 10.1038/srep41848

Morell M, Lenoir M, Shadwick RE, et al (2015) Ultrastructure of the Odontocete Organ of Corti: Scanning and transmission electron microscopy. J Comp Neurol 523:431–448. doi: 10.1002/cne.23688

Müller M (1991) Frequency representation in the rat cochlea. Hear Res 51:247–254

Müller M, Von Hünerbein K, Hoidis S, Smolders JWT (2005) A physiological place-frequency map of the cochlea in the CBA/J mouse. Hear Res 202:63–73. doi: 10.1016/j.heares.2004.08.011

Ni G, Elliott SJ, Baumgart J (2016) Finite-element model of the active organ of Corti. J R Soc Interface 13:. doi: 10.1098/rsif.2015.0913

Pau HW, Pau H (2006) Does the geometrical arrangement of the outer hair cell stereocilia perform a fluid-mechanical function? Acta Otolaryngol 126:570–576. doi: 10.1080/00016480500468992

Pujol R, Lenoir M, Ladrech S, et al (1992) Correlation between the length of outer hair cells and the frequency coding of the cochlea. In: Cazals Y, Horner K, Demany L (eds) Auditory Physiology and Perception. Pergamon, pp 45–52

R Core Team (2018) R: A language and environment for statistical computing

Raphael Y, Altschuler RA (2003) Structure and innervation of the cochlea. Brain Res Bull 60:397–422. doi: 10.1016/S0361-9230(03)00047-9

Rhode WS, Recio A (2000) Study of mechanical motions in the basal region of the chinchilla cochlea. J Acoust Soc Am 107:3317–3332. doi: 10.1121/1.429404

Rohlf FJ (2004a) TPSUtil, Version 1.70

Rohlf FJ (2004b) TPSDig2, Version 2.26

Schneider CA, Rasband WS, Eliceiri KW (2012) NIH Image to ImageJ: 25 years of image analysis. Nat Methods 9:671–675. doi: 10.1038/nmeth.2089

Schweitzer L, Lutz C, Hobbs M, Weaver SP (1996) Anatomical correlates of the passive properties underlying the developmental shift in the frequency map of the mammalian cochlea. Hear Res 97:84–94

Spicer SS, Schulte BA (1994) Differences along the place-frequency map in the structure of supporting cells in the gerbil cochlea. Hear Res 79:161–177

Strelioff D, Flock Å, Minser KE (1985) Role of inner and outer hair cells in mechanical frequency selectivity of the cochlea. Hear Res 18:169–175

Vater M, Kössl M (2011) Comparative aspects of cochlear functional organization in mammals. Hear Res 273:89–99. doi: 10.1016/j.heares.2010.05.018

Vater M, Kössl M (1996) Further studies on the mechanics of the cochlear partition in the mustached bat. I. Ultrastructural observations on the tectorial membrane and its attachments. Hear Res 94:63–77. doi: 10.1016/0378-5955(96)00005-6

Vater M, Lenoir M (1992) Ultrastructure of the horseshoe bat's organ of Corti. I. Scanning electron microscopy. J Comp Neurol 318:367–379

Vater M, Siefer W (1995) The cochlea of *Tadarida brasiliensis*: specialized functional organization in a generalized bat. Hear Res. doi: 10.1016/0378-5955(95)00188-3

Von Békésy G (1960) Experiments in Hearing. McGraw-Hill

Wright A (1984) Dimensions of the cochlear stereocilia in man and the guinea pig. Hear Res 13:89–98

Yao Q, Zeng JY, Zheng YM, et al (2007) Characteristics of echolocating bats' auditory stereocilia length, compared with other mammals. Sci China, Ser C Life Sci 50:492–496. doi: 10.1007/s11427-007-0055-8

Yarin YM, Lukashkin AN, Poznyakovskiy AA, et al (2014) Tonotopic morphometry of the lamina reticularis of the guinea pig cochlea with associated microstructures and related mechanical implications. JARO - J Assoc Res Otolaryngol 15:1–11. doi: 10.1007/s10162-013-0420-1

Supplementary Table 1. Geometric morphometrics – landmark descriptions

	Landmark number	Description
IHC	1	leftmost middle point of the first IHC
	2	rightmost middle point of the first IHC
	3	upper middle point of the first IHC
	4	lower middle point of the first IHC
	5	leftmost middle point of the second IHC
	6	rightmost middle point of the second IHC
	7	upper middle point of the second IHC
	8	lower middle point of the second IHC
	9	leftmost middle point of the third IHC
	10	rightmost middle point of the third IHC
	11	upper middle point of the third IHC
	12	lower middle point of the third IHC
OHC1	13	leftmost point of the first OHC1 in line with the end of the stereocilia
	14	rightmost point of the first OHC1 in line with the end of the stereocilia
	15	upper middle point of the first OHC1 in line with the W
	16	lower middle point of the first OHC1 in line with the W
	17	leftmost point of the second OHC1 in line with the end of the stereocilia
	18	rightmost point of the second OHC1 in line with the end of the stereocilia
	19	upper middle point of the second OHC1 in line with the W
	20	lower middle point of the second OHC1 in line with the W
	21	leftmost point of the third OHC1 in line with the end of the stereocilia
	22	rightmost point of the third OHC1 in line with the end of the stereocilia
	23	upper middle point of the third OHC1 in line with the W
	24	lower middle point of the third OHC1 in line with the W

	Landmark number	Description
OHC2	25	leftmost point of the first OHC2 in line with the end of the stereocilia
	26	rightmost point of the first OHC2 in line with the end of the stereocilia
	27	upper middle point of the first OHC2 in line with the W
	28	lower middle point of the first OHC2 in line with the W
	29	leftmost point of the second OHC2 in line with the end of the stereocilia
	30	rightmost point of the second OHC2 in line with the end of the stereocilia
	31	upper middle point of the second OHC2 in line with the W
	32	lower middle point of the second OHC2 in line with the W
	33	leftmost point of the third OHC2 in line with the end of the stereocilia
	34	rightmost point of the third OHC2 in line with the end of the stereocilia
	35	upper middle point of the third OHC2 in line with the W
	36	lower middle point of the third OHC2 in line with the W
OHC3	37	leftmost point of the first OHC3 in line with the end of the stereocilia
	38	rightmost point of the first OHC3 in line with the end of the stereocilia
	39	upper middle point of the first OHC3 in line with the W
	40	lower middle point of the first OHC3 in line with the W
	41	leftmost point of the second OHC3 in line with the end of the stereocilia
	42	rightmost point of the second OHC3 in line with the end of the stereocilia
	43	upper middle point of the second OHC3 in line with the W
	44	lower middle point of the second OHC3 in line with the W
	45	leftmost point of the third OHC3 in line with the end of the stereocilia
	46	rightmost point of the third OHC3 in line with the end of the stereocilia
	47	upper middle point of the third OHC3 in line with the W
	48	lower middle point of the third OHC3 in line with the W

Supplementary Table 2. Summary of results from the statistical analyses for linear morphometric measurements from 19 parameters in Parnell's mustached bat (n = 6) and rats (n = 4) plus stereocilia length in the bats. (a) Results between the apex and base in bats. (b) Results from the fovea region to base in bats (measured from 35 - 50%, 50 - 70%, and 70 - 100%) for the parameters cuticular plate width (CW), distance between stereociliary bundle tips (SBD), and stereociliary bundles - inner angle (SBA). (c) Results from the stereocilia in bats. (d) Results between the apex and base in rats.

(a) Results for normality using a Shapiro-Wilk test. If p-value < 0.05 the data is not normal, if else it is normal.

Parameter Abbreviation	Measurement	Shapiro-Wilks P-value	Shapiro-Wilks Statistic W	Shrapiro-Wilks Normality	Secondary Test Used	P-value	Statistic W or T	Difference Between Apex and Base
RLW	IHC - OHC3	1.67E-03	0.9348708	Non normal	Wilcoxon-Test	7.31E-12	W = 1066	Significant
RD1	IHC - OHC1	7.38E-03	0.9482036	Non normal	Wilcoxon-Test	7.40E-19	W = 1066	Significant
RD2	OHC1 - OHC2	7.20E-02	0.9669869	Normal	T-Test	5.41E-19	T = 13.08	Significant
RD3	OHC2 - OHC3	2.49E-05	0.8907899	Non normal	Wilcoxon-Test	7.30E-12	W = 1066	Significant
CL1	OHC1 CP length	5.47E-02	0.9647871	Normal	T-Test	6.33E-04	T = 3.66	Significant
CL2	OHC2 CP length	3.79E-02	0.9618327	Non normal	Wilcoxon-Test	9.16E-07	W = 915	Significant
CL3	OHC3 CP length	3.50E-02	0.961189	Non normal	Wilcoxon-Test	3.85E-10	W = 1020	Significant
CW1	OHC1 CP width	1.35E-03	0.9328688	Non normal	Wilcoxon-Test	8.88E-11	W = 28.50	Significant
CW2	OHC2 CP width	1.58E-01	0.9732514	Normal	T-Test	5.91E-09	T = -6.85	Significant
CW3	OHC3 CP width	1.05E-01	0.9699841	Normal	T-Test	4.00E-12	T = -9.01	Significant
SBD1	Bundle Tips OHC1 distance	8.53E-04	0.9285082	Non normal	Wilcoxon-Test	5.93E-01	W = 491	No difference
SBD2	Bundle Tips OHC2 distance	4.98E-04	0.9232357	Non normal	Wilcoxon-Test	9.23E-01	W = 525	No difference
SBD3	Bundle Tips OHC3 distance	8.11E-03	0.9490178	Non normal	Wilcoxon-Test	9.23E-01	W = 496.5	No difference
GW1	Gap Width OHC1	4.72E-06	0.8702633	Non normal	Wilcoxon-Test	7.29E-12	W = 1066	Significant
GW2	Gap Width OHC2	9.19E-06	0.8787143	Non normal	Wilcoxon-Test	3.51E-09	W = 992.5	Significant
GW3	Gap Width OHC3	5.57E-04	0.9243463	Non normal	Wilcoxon-Test	1.98E-10	W = 1028	Significant
SBA1	Angle OHC1	4.60E-04	0.9224392	Non normal	Wilcoxon-Test	1.48E-18	W = 1	Significant
SBA2	Angle OHC2	4.58E-04	0.9223952	Non normal	Wilcoxon-Test	7.31E-12	W = 0	Significant
SBA3	Angle OHC3	1.42E-05	0.8840266	Non normal	Wilcoxon-Test	7.40E-19	W = 0	Significant

* Note: In the Apex group, n = 41; Base group, n = 26

(b) Results for normality using a Shapiro-Wilk test. If p-value < 0.05 the data is not normal, if else it is normal.

Parameter Abbreviation	Measurement	Shapiro-Wilks P-value	Shapiro-Wilks Statistic W	Shrapiro-Wilks Normality	Secondary Test Used	P-value	Statistic KW	Degrees of Freedom (df)	Difference	Post-hoc Dunn's Test Required
CW	OHC CP Width Average 1, 2, 3	2.01E-08	0.9134038	Non normal	Kruskal-Wallis Test	6.05E-02	KW = 5.61	2	No difference	No
SBD	Bundle Tips OHC Distance Average 1, 2, 3	8.20E-06	0.9484137	Non normal	Kruskal-Wallis Test	1.52E-03	KW =12.98	2	Significant	Yes
SBA	Angle OHC; Average 1, 2, 3	3.34E-02	0.9825785	Non normal	Kruskal-Wallis Test	2.53E-04	KW =16.56	2	Significant	Yes

Dunn's Test Results:

		Kruskal-Wallis rank sum test (data: y and x)			Dunn's Test Results			
		Chi-squared	Degrees of Freedom (df)	P-value	Comparison	Result	P-value	Z
SBD	Bundle Tips OHC Distance Average 1, 2, 3	12.9821	2	0	[35%-50%] - [50%-70%]	Difference	0.0048692	-2.8155628
					[35%-50%] - [70-100%]	Difference	0.0012448	-3.3426439
					[50%-70%] - [70-100%]	No difference	0.3652158	0.3445516
SBA	Angle OHC; Average 1, 2, 3	16.5645	2	0	[35%-50%] - [50%-70%]	Difference	0.0040818	-2.87176765
					[35%-50%] - [70-100%]	Difference	0.0001308	-3.92375764
					[50%-70%] - [70-100%]	No difference	0.4709356	-0.07291821

* Note: In the [35%-50%] group, n=48; [50%-70%] group, n=28; [70-100%] group, n=92

(c) Results for normality using a Shapiro-Wilk test. If p-value < 0.05 the data is not normal, if else it is normal.

Measurement	Shapiro-Wilks P-value	Shapiro-Wilks Statistic W	Shrapiro-Wilks Normality	Secondary Test Used	P-value	Statistic W or T	Difference Between Apex and Base
Stereocilia Length OHC1	5.23E-08	0.8693489	Non normal	Wilcoxon-Test	4.94E-12	W = 1640	Significant
Stereocilia Length OHC2	1.30E-10	0.7947933	Non normal	Wilcoxon-Test	4.94E-12	W = 1640	Significant
Stereocilia Length OHC3	3.06E-05	0.9275691	Non normal	Wilcoxon-Test	4.94E-12	W = 1640	Significant

* Note: In the Apex group, n = 82; Base group, n = 20; The Wilcoxon-Test was a Wilcoxon rank sum test with continuity correction

(d) Results for normality using a Shapiro-Wilk test. If p-value < 0.05 the data is not normal, if else it is normal.

Parameter Abbreviation	Measurement	P-value	Statistic W	Normality	Secondary Test Used	P-value	Statistic W or T	Difference Between Apex and Base
RLW	IHC - OHC3	5.55E-06	0.6911553	Non normal	Wilcoxon-Test	3.58E-05	W = 150	Significant
RD1	IHC - OHC1	1.80E-05	0.7284556	Non normal	Wilcoxon-Test	3.56E-05	W = 150	Significant
RD2	OHC1 - OHC2	3.39E-05	0.7473847	Non normal	Wilcoxon-Test	6.12E-07	W = 150	Significant
RD3	OHC2 - OHC3	9.93E-05	0.7778554	Non normal	Wilcoxon-Test	3.51E-05	W = 150	Significant
CL1	OHC1 CP length	3.25E-04	0.8092348	Non normal	Wilcoxon-Test	6.12E-07	W = 150	Significant
CL2	OHC2 CP length	1.57E-03	0.8474277	Non normal	Wilcoxon-Test	3.58E-05	W = 150	Significant
CL3	OHC3 CP length	6.92E-02	0.9256979	Normal	T-Test	6.55E-10	T = 11.17	Significant
CW1	OHC1 CP width	6.58E-01	0.9704894	Normal	T-Test	1.81E-04	T = -4.75	Significant
CW2	OHC2 CP width	1.48E-01	0.9399584	Normal	T-Test	1.34E-01	T = -1.59	No difference
CW3	OHC3 CP width	2.52E-01	0.9500782	Normal	T-Test	4.42E-01	T = -0.80	No difference
SBD1	Bundle Tips OHC1 distance	5.41E-01	0.9657661	Normal	T-Test	5.55E-01	T = -0.60	No difference
SBD2	Bundle Tips OHC2 distance	1.18E-01	0.9357332	Normal	T-Test	3.32E-01	T = 1.00	No difference
SBD3	Bundle Tips OHC3 distance	3.64E-01	0.9573239	Normal	T-Test	3.15E-01	T = 1.04	No difference
GW1	Gap Width OHC1	4.50E-04	0.8173874	Non normal	Wilcoxon-Test	6.12E-07	W = 150	Significant
GW2	Gap Width OHC2	9.32E-04	0.8351361	Non normal	Wilcoxon-Test	6.12E-07	W = 150	Significant
GW3	Gap Width OHC3	2.19E-03	0.854905	Non normal	Wilcoxon-Test	3.56E-05	W = 150	Significant
SBA1	Angle OHC1	2.74E-03	0.8599374	Non normal	Wilcoxon-Test	6.12E-07	W = 0	Significant
SBA2	Angle OHC2	6.78E-03	0.8796066	Non normal	Wilcoxon-Test	6.12E-07	W = 0	Significant
SBA3	Angle OHC3	2.92E-03	0.8613771	Non normal	Wilcoxon-Test	6.12E-07	W = 0	Significant

*Note: In the Apex group, n = 15; Base group, n = 10